ACS OMEGA

Open Access

http://pubs.acs.org/journal/acsodf

Article

Synthesis, Structural Characterization, and Computational Studies of Novel Co(II) and Zn(II) Fluoroquinoline Complexes for Antibacterial and Antioxidant Activities

Tadewos Damena,* Tegene Desalegn, Sadhna Mathura, Alemayehu Getahun, Dereje Bizuayehu, Mamaru Bitew Alem, Shiferaw Gadisa, Digafie Zeleke, and Taye B. Demissie

Cite This: *ACS Omega* 2024, 9, 36761−36777

Read Online

ACCESS | Metrics & More | Article Recommendations | Supporting Information

ABSTRACT: Research into heterocyclic ligands has increased in popularity due to their versatile applications in the biomedical field. Quinoline derivatives with their transition metal complexes are popular scaffolding molecules in the ongoing pursuit of newer and more effective bioactive molecules. Subsequently, this work reports on the synthesis and possible biological application of new Zn(II) and Co(II) complexes with a bidentate quinoline derivative ligand (H_2L), [(H_2L):(*E*)-2-(((6-fluoro-2-((2-hydroxyethyl)amino)quinolin-3-yl)methylene)amino)ethanol]. The ligand and its metal complexes were structurally characterized by spectroscopic methods (^{1}H NMR, ^{13}C NMR, Fourier transform infrared (FTIR), UV−vis, fluorescence, and mass spectroscopy), as well as by thermogravimetric and elemental analysis methods. The spectroscopic findings were further supported by density functional theory (DFT) and time-dependent (TD)-DFT calculations. The biological application was examined by investigating the inhibitory action of the complexes against bacterial strains using diffusion and agar dilution methods, and their profiles against two Gram-positive and Gram-negative bacterial strains were supported by molecular docking analysis. To rationalize the *in vitro* activity and establish the possible mechanism of action, the interactions and binding affinity of the ligand and complexes were investigated against three different bacterial enzymes (*Escherichia coli* DNA gyrase (PDB ID 6f86), *E. coli dihydrofolate* reductase B (PDB ID: 7r6g), and *Staphylococcus aureus* tyrosyl-tRNA synthetase (PDB ID: 1JIJ)) using AutoDock with the standard protocol. The MIC value of 0.20 μg/mL for zinc complex against *E. coli* and associated binding affinities −7.2 and −9.9 kcal/mol with *DNA* gyrase (PDB ID 6f86) and *dihydrofolate reductase* B (PDB ID: 7r6g), as well as the MIC value of 2.4 μg/mL for cobalt(II) complex against *Staphylococcus aureus* and the associated binding affinity of −10.5 kcal/mol with *tyrosyl-tRNA synthetase* (PDB ID: 1JIJ), revealed that the complexes' inhibitory actions were strong and comparable with those of the standard drug in the experiments. In addition, the ability of the new quinoline-based complexes to scavenge 1,1-diphenyl-picrylhydrazyl radicals was investigated; the findings suggested that the complexes exhibit potent antioxidant activities, which may be of therapeutic significance.

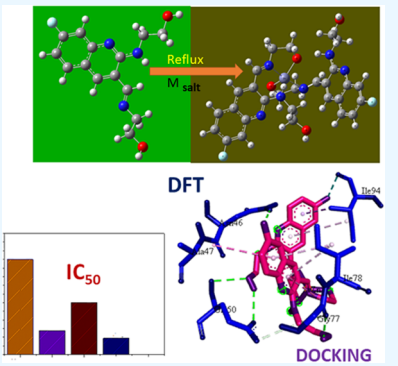

1. INTRODUCTION

Quinoline (C_9H_7N) or 1-aza-naphthalene or benzo[*b*]pyridine is a heterocyclic aromatic compound in which 10π electrons are delocalized throughout the structure. These organic compounds are structurally heterobicyclic, having a benzene ring fused to pyridine.[1,2] This structural motif allows quinoline derivatives to serve as popular building blocks in medicinal chemistry.[1,3−5] Quinoline and its substituted derivatives represent the major class of heterocycles known to have well-established synthetic routes since the late 1800s.[4−6] They have both natural and synthetic origins, which are classified based on structural modification as well as biological activity.[1−5] Quinoline-based heterocyclic derivative scaffolds are known to exhibit excellent properties toward communicable[3,7] and noncommunicable[1,5,6] disease. Their broad spectrum of biological and biochemical activities have been further aided by the synthetic flexibility of quinoline derivatives, which allows the generation of a large number of structurally diverse derivatives and their metal-based complexes.[8] These compounds possess the ability to coordinate strongly to metal ions, yielding complexes that incorporate diverse geometries, as well as different coordination modes with the most common coordination mode being the bidentate or tridentate chelation through the carbonyl, phenolato oxygen, and their substituted imine nitrogen atoms.[8−10]

The study of the biological activity of coordination compounds with biologically active metals and N and O atom donor bioactive ligands is at the forefront of the field of coordination chemistry. It has been found that the activities of

Received: June 17, 2024
Revised: July 24, 2024
Accepted: July 30, 2024
Published: August 15, 2024

these bioactive molecules can be enhanced upon their coordination to different biologically active metals, like copper, zinc, cobalt, nickel, iron, and vanadium.[9−15] Metal complexes, due to their specific and unique physicochemical properties, have been proven to be very convenient in the development of new therapeutic agents for clinical use. The variety of coordination numbers, geometry, ligand flexibility, and redox activity combined with the biological properties of the metal ions may give rise to many possibilities for the design of therapeutic agents that cannot be found in organic ligands.[16,17]

Antimicrobial resistance has become public health emergency, and it seems that organic chemistry alone is not adequate to supply the world with new effective antimicrobial agents.[18]

In the last few decades, a renewed interest in metal-based therapy has been raised; in fact, on coordination, not only bioactive ligands might improve their bioactivity profiles but also inactive ligands may acquire pharmacological properties. In this regard, the heterocyclic quinoline constitutes are an important class of biologically active ligand molecules that have attracted the attention of bioinorganic and medicinal chemists due to their versatile coordination behavior and a wide range of pharmacological properties.[19−21]

It is known that the active sites of metalloenzymes (carbonic anhydrase, superoxide dismutase, cobalamin, and hemoglobin) can function with the help of transition metal ions (Zn, Cu, Co, Fe) respectively. Therefore, the synthesis of metal complexes can be used to simulate the active centers to assist in the biological activity of organic compounds.[22] One of the main characteristics of transition metal ions is their potential to undergo redox processes and their ability to switch between several oxidation states due to the redox activity of metals. Researchers have synthesized and characterized different metal complexes based on heterocyclic quinoline derivatives as antibacterial and antioxidant agents with VO^{2+}, Mn^{2+}, Fe^{2+}, Co^{2+}, Ni^{2+}, Zn^{2+}, MoO_2^{2+}, Cd^{2+}, and UO_2^{2+}[23−26] Even though organic drugs have traditionally dominated modern medicinal chemistry and pharmacology, inorganic medicinal chemistry has become a growing research area whose current development has been triggered by the discovery of cisplatin as an antitumor agent. In this research work, we have focused on the preparation of Co and Zn complexes with a heterocyclic quinoline derivative ligand. We have tried to elucidate the structure of newly synthesized complexes with help of a quantum chemical approach (density functional theory (DFT) and time-dependent (TD)-DFT) to support experimental results. The pharmacological behavior of newly synthesized complexes was then investigated to explore the antibacterial activities against four human pathogenic bacteria: *Escherichia coli* (*E. coli*), *Pseudomonas aeruginosa* (*P. aeruginosa*), *Staphylococcus aureus* (*S. aureus*), and *Streptococcus pyogenesis* (*S. pyogenesis*). The binding potential and the mode of interactions of the complexes with the sequence of amino acids of proteins of *E. coli* and *S. aureus* were also assessed. In addition, the proper orientation of the complexes buried inside of the disease-carrying active sites of a pathogenic, contagious, and drug-resistant bacteria protein is also verified by employing the *in silico* approach..[27,28]

2. MATERIALS AND METHODS

2.1. Chemicals and Reagents. The chemicals and reagents used for this study were acetic anhydride 99.8%, acetic acid glacial 99.5%, aniline 99%, zinc dust 95%, *N*,*N*-dimethylformamide 99%, phosphoryl chloride 98%, methanol 99.5%, trimethylamine 99%, *n*-Hexane 99%, dichloromethane 98%, ethyl acetate 99.5%, cobalt chloride hexahydrate 98%, zinc chloride 98%, ascorbic acid 99%, dimethyl sulfoxide 99%, 2,2-diphenyl-1-picrylhydrazyl (DPPH), and silver nitrate 99.9%. All of the chemicals and reagents were purchased from Loba Chemie PVT. LtD (Mumbai, India) and were of analytical grade and used without further purification.

2.2. Instruments and Apparatus. ^{1}H NMR and ^{13}C NMR spectra were recorded using a Bruker Avance III 500 MHz instrument in d_6-DMSO using tetramethylsilane (TMS) as an internal reference. Elemental composition was analyzed using an elemental analyzer (Thermoscientific FlashSmart CHNS/O). Fluorescence spectra were recorded using Agilent MY-18490002/PC spectrofluorophotometer. Mass spectra were recorded with SHIMADZU LC-MS (8030). The UV−visible spectral data were recorded on a SM-1600 spectrophotometer. Fourier transform infrared (FTIR) data were recorded with PerkinElmer BX spectrometer (4000−400 cm^{-1}) using KBr pellets. Thermogravimetric analyses (TGA) and differential thermal analysis (DTA) were performed under N_2 atmosphere (20 mL/min) using the detector DTG-60H Shimadzu thermal analyzer. The rate of heating of the sample was accomplished at 10 °C/min, between 25 to 800 °C. Molar conductivity was measured using an electrical conductometer (AD8000). Melting point was measured using capillary tubes with a digital melting point detector. Thin-layer chromatography (TLC) was run on a 0.2 mm silica gel GF254 (Merck) on an aluminum plate and spots were detected using UV light (254 and 366 nm).

2.3. Synthesis of the Ligand [(*E*)-2-(((6-Fluoro-2-((2-hydroxyethyl)amino)quinolin-3-yl)methylene)amino)-ethanol (H_2L)]. The ligand was prepared following previously reported procedures[2,3,29] with some modification. Accordingly, 2-chloro-6-fluoroquinoline-3-carbaldehyde (3.5 g, 0.017 mol) was added to 10 mL of 2-aminoethan-1-ol in a 250 mL round-bottom flask, and the mixture was heated at 100 °C for 2 h in an oil bath. The reaction progress was monitored using TLC. When the reaction was completed, the resultant mixture was cooled to room temperature and then added to ice-cold water (100 mL) to precipitate the ligand. The white precipitate was then separated by suction filtration and washed with a further 200 mL of ice-cold water. Finally, the ligand was dried at room temperature for several days.

2.4. Synthesis of Transition Metal Complexes. *2.4.1. Synthesis of Zinc(II) Complex (**1**).* Under constant stirring at room temperature, a drop of trimethylamine (TEA) was added to 20 mL of methanolic solution of the ligand (0.27 g, 0.974 mmol) in 200 mL two-neck round-bottom flask. After 30 min of stirring, 20 mL of a methanolic solution of $ZnCl_2$ (0.07 g, 0.487 mmol) was added dropwise to the ligand solution, under continuous stirring, and then the mixture was refluxed for 4 h at 90 °C in an oil bath.[15,19,20] The reaction progress was monitored by TLC and when the reaction was completed, the resultant mixture was cooled to room temperature and then filtered by suction filtration. The precipitate was washed with cold methanol and then dried at room temperature[9] for several days.

*2.4.2. Synthesis of Cobalt(II) complex (**2**).* A methanolic solution of the ligand (0.27 g, 0.974 mmol) (20 mL) was mixed with a drop of TEA under constant pressure at room temperature. Then after, 20 mL of a warm methanolic solution of cobalt chloride hexahydrate ($CoCl_2{\cdot}6H_2O$) (0.116 g, 0.487 mmol) was added dropwise to the solution of the ligand under constant stirring and were refluxed for 4 h at 90 °C, under inert atmosphere, and the reaction progress was monitored by TLC. When the reaction was completed, the resultant mixture was

https://doi.org/10.1021/acsomega.4c05560
ACS Omega 2024, 9, 36761−36777

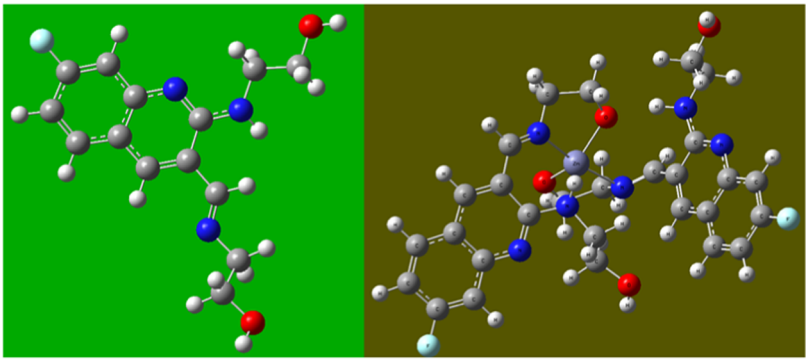

Figure 1. Optimized structure of the ligand and complex **1**.

cooled to room temperature and then filtered using suction filtration. The precipitate was washed with cold methanol before being dried at ambient temperature[10,20,21,30] for several days.

2.5. Computational Studies. *2.5.1. DFT Calculations.* Geometric optimizations of the ligand and its metal complexes were performed using the Gaussian 16 program package[31] and the results were visualized using Gauss View 06[32] (Figure 1) and Chemcraft.[33] The Density Functional Theory (DFT) and time-dependent DFT (TD-DFT) calculations were performed using the B3LYP hybrid functional, which together with the 6-311++G(d,p) basis set was utilized for the light atoms[34] and the LanL2DZ basis sets were utilized for the metal atoms to account for relativistic effects. The optimized geometries were confirmed to be real minima without any imaginary vibrational frequencies by performing vibrational frequency calculations at the same level of theory. Grimme's dispersion correction was employed to treat nonbonding interactions during the calculations[35] and, to mimic the experimental conditions, the polarizable continuum model in its integral equation formalism (IEF-PCM) together with the methanol solvent was employed to correct the solvent effects. The Eigen values of the highest occupied molecular orbital (HOMO) and lowest unoccupied molecular orbital (LUMO) and their wave function distributions were calculated and visualized. Quantum chemical descriptors such as band gap energy ($E_g = E_{LUMO} - E_{HOMO}$), electronegativity ($\chi = -1/2(E_{HOMO} + E_{LUMO})$), electronic chemical potential ($\mu = 1/2(E_{HOMO} + E_{LUMO}) = -\chi$), global chemical hardness ($\eta = 1/2(E_{LUMO} - E_{HOMO})$), global softness ($\sigma = 1/2\eta$), global electrophilicity index ($\omega = \mu^2/2\eta$), nucleophilicity index ($Nu = 1/\omega$), and dipole moment were calculated and analyzed at the same level of theory.[9,32]

2.5.2. Molecular Docking Studies. The interactions and binding affinity of the ligand and its complexes were investigated against three different bacterial enzymes using AutoDock with a standard protocol.[36] The three different enzymes examined were *E. coli* DNA gyrase (PDB ID 6f86), *E. coli dihydrofolate reductase* B (PDB ID: 7r6g), and *S. aureus tyrosyl-tRNA synthetase* (PDB ID: 1JIJ). Crystal structures of the three enzymes were downloaded from Protein Data Bank.[37−39] The proteins were processed using Discovery Studio 2024 and Autodock tools 1.5.6.[36,40] The active sites of the enzymes were taken from the attributes of SPD Sphere of the corresponding enzyme, which were *x,y,z* = 61.680259, 28.330852, 64.290148, radius = 10.105432 for 6F86; *x,y,z* = 10.093469, −53.275716, −7.239296, radius = 10.093469, −53.275716, −7.239296 for 7RG6; and *x,y,z* = −11.639999, 17.310547, 91.728918, radius = 38.148403 for 1JIJ. Chem Office tools (Chemdraw ultra 12.0 2D and 3D) were used to prepare the energy-minimized chemical structures of the ligand and complexes; Open Babel GUI was used to convert the images of the ligand and complexes into their different file formats. The enzymes' images were prepared by removing water and cocrystallized ligand, and by adding polar hydrogen and charges.[3,9,41] Nine different conformers were considered for the docking process of the ligands and complexes; in each case, the least free binding energy conformations of the ligand or complex was selected for analyzing the interactions of the residue in the receptor enzyme with the ligand and complexes. The Discovery Studio Visualizer was used to represent 3D and 2D residual interaction in stick model representation with the enzymes.[9,21,37,38]

2.6. Biological Activity Analysis. *2.6.1. Antibacterial Activity of the Ligand and Its Metal Complexes.* The antibacterial activities of the ligand and the metal complexes were examined using human pathogenic Gram-negative (*E. coli* and *P. aeruginosa*) and Gram-positive (*S. aureus* and *S. pyogenes*) bacterial strains. These activities were examined by exploiting two methods: (I) paper disc diffusion and (II) agar dilution methods.

I. Paper disc diffusion method. The medium was prepared from molten nutrient and Mueller−Hinton agar. Ciprofloxacin and DMSO were used as positive and negative controls, respectively. The bacterial strains were tested against two compound concentrations (100 and 200 μg/mL), prepared by dissolving appropriate amounts of the compound into DMSO to form a solution. Whatman filter paper discs (6 mm) were then soaked in 1 mL samples of each solution. These saturated paper discs were then inoculated at the center of a Petri dish having the bacterial lawn in triplicate. The plates were incubated at 37 °C for 48 h. The inhibition zone was determined by measuring the diameter of the inhibition zone.[2,9,10,20,42] The bacterial activities of the synthesized complexes were confirmed by calculating the percent activity index (AI),[20] eq 1.

$$\%\ \text{Activity index (AI)} = \frac{\text{Mean inhibition zone of compounds}}{\text{Mean inhibition zone of standard}} \times 100 \quad (1)$$

II. Broth Dilution Methods. Three common broth dilution methods are used for antimicrobial testing: agar diffusion, agar dilution, and bioautographic methods.[43] Determination of the minimum inhibitory concentration (MIC) with the dilution method is considered as more reliable and reproducible than the agar diffusion method.[44] Thus, to examine the reproducibility of the antibacterial assay, in addition to the mean inhibition zone (MIZ), the MIC of the complexes was determined using agar dilution assay for the above four bacteria strains using a

https://doi.org/10.1021/acsomega.4c05560
ACS Omega 2024, 9, 36761−36777

Table 1. Physicochemical Properties of the Ligand and Transition Metal Complexes[a]

compounds	color	yield (%)	melting point (°C)	conductivity (Ω^{-1} mol^{-1} cm^2 25 °C)
$C_{14}H_{17}FN_3O_2$ (**H_2L**)	yellow	87	65−70	
$[Zn(HL)_2]$ (**1**)	light yellow	68	205−210	8.30 ± 0.31
$[Co(HL)_2(H_2O)_2]$ (**2**)	deep brownish	65	255−260	10.36 ± 0.42

[a]**Note:** [$C_{14}H_{17}FN_3O_2$ (Ligand) = **H_2L**], [**HL** = deprotonated ligand]; **1** = Complex **1**; **2** = Complex **2**.

Scheme 1. Synthesis of *N*-(4-fluorophenyl)acetamide from Aniline[29]

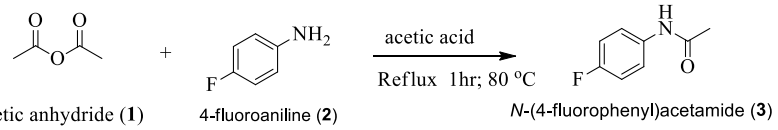

Acetic anhydride (**1**) 4-fluoroaniline (**2**) *N*-(4-fluorophenyl)acetamide (**3**)

Scheme 2. Synthesis of Vilsmeier Reagent[2,3,29]

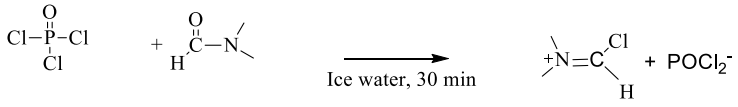

Phosphorus oxychloride (**4**) N,N-dimethyl formamide (**5**) [Vilsmeier reagent (**6**)]

Scheme 3. Synthesis of 2-Chloro-6-fluoroquinoline-3-carbaldehyde[29]

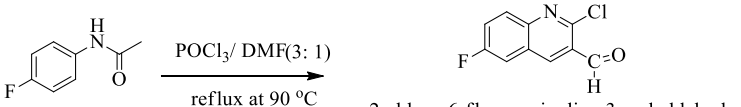

N-(4-fluorophenyl)acetamide (**3**) 2-chloro-6-fluoroquinoline-3-carbaldehyde

previously reported method.[2,3,9,10] Bacterial suspension was prepared by inoculating the nutrient broth with a loopful of each of the four bacterial cultures from the slant and incubating at 37 ± 1 °C until the growth reached a turbidity equal to a 0.50 McFarland standard. Freshly sterilized broth (20 mL) was then seeded with 0.25 to 0.30 mL of the above broth cultures to give a final organism density close to 5×10^5 CFU/mL. At the same time, 1 mg/mL (1000 μg/mL) stock solutions were prepared by dissolving 50 mg of each complex, the ligand, and ciprofloxacin in 50 mL of sterile distilled water. The first dilution of each antimicrobial agent was prepared in test tubes by adding 0.26 mL of each antimicrobial agent to 4.73 mL of the seeded broth, which afforded a 51.2 μg/mL solution. Then, for each of the above antimicrobial agents, 12 different 2 mL dilutions (51.2, 25.6, 12.8, 6.4, 3.2, 1.60, 0.80, 0.40, 0.20, 0.10, 0.050, and 0.025 μg/mL) were prepared for each of the bacterial strains by a 2-fold serial dilution method using a micropipette. The ciprofloxacin-containing tubes were used as a positive control, whereas bacterial seeded broths with pure DMSO were used as a negative control. All of the prepared solutions were incubated at 37 ± 1 °C for 24 h and the lowest concentration of the antimicrobial agent that prevented the appearance of visible growth of microorganisms was taken as its MIC value.[45−47]

2.6.2. Antioxidant Activity of the Compounds. The antioxidant activities of the ligand and its complexes were systematically assessed using the 1,1-diphenyl-picrylhydrazyl (DPPH) test, a standard method for evaluating the capability of compounds to remove free radical materials.[48] The DPPH radical scavenging effectiveness of both the ligand and its respective complexes were quantified spectrophotometrically by monitoring the reduction of DPPH in methanol solution. To initiate the process, 11 different concentrations of the compounds were prepared based on the previous reported studies.[9,10,48] In the experimental process, 1 mL of DPPH solution was added into each 1 mL sample of the synthesized compounds in methanol. The control was prepared by adding 1 mL of the DPPH solution to 1 mL of methanol, while 2 mL of methanol was used as a blank. Subsequently, each of these solutions were introduced into individual wells of a microplate and the resultant mixture was shaken vigorously. The prepared solutions were incubated (Labfreez: TSI-200) at 37 °C in the dark for 30 min before the absorbance data were recorded. Absorbance data were recorded at 517 nm using a double-beam UV−vis spectrophotometer; then, the quenching of the absorbance at 517 nm was examined at a constant time of 30 min and Vitamin C was used as a positive control. All of the activities were performed in triplicate and the average absorbance was taken for percentage inhibition calculation using eq 2:

$$\text{DPPH}_{\text{radical scavenging activity (\%)}} = \left[\frac{(A_i - A_s)}{A_i}\right] \times 100\% \quad (2)$$

where A_i and A_S are the absorbances of the control and sample with control solution, respectively. Finally, the half-maximal inhibitory concentration (IC_{50}) was determined from the slope and intercept of the plot of percent radical scavenging activity vs concentration.

2.7. Statistical Analysis. The antibacterial experimental measurements were collected in triplicate (reported as means with standard deviations). Statistical analyses were completed using GraphPad Prism version 5.00 for Windows (GraphPad Software, San Diego, California).[49] Groups were analyzed for significant differences using a linear model of variance analysis (ANOVA) test for comparisons with significance accepted for $p < 0.05$.

https://doi.org/10.1021/acsomega.4c05560
ACS Omega 2024, 9, 36761−36777

Scheme 4. Proposed Synthesis and Reaction Mechanisms of the Ligand[29]

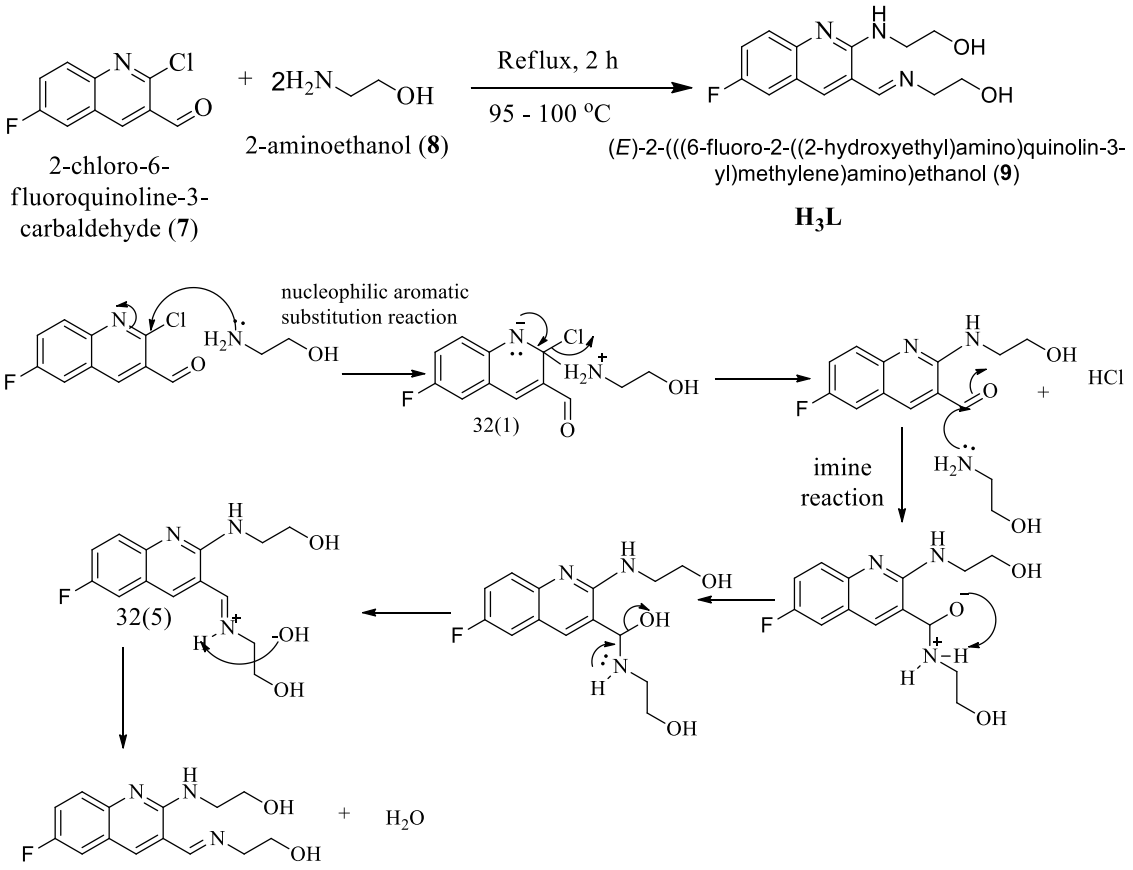

3. RESULTS AND DISCUSSION

3.1. Synthesis of the Ligand and Its Transition Metal Complexes. The preparation of the ligand and the corresponding metal complexes was performed by following the established procedures outlined in Section 2. The ligand ($\mathbf{H_2L}$), (*E*)-2-(((6-fluoro-2-((2-hydroxyethyl)amino)quinolin-3-yl)methylene)-amino)ethanol, was prepared from 2-chloro-6-fluoroquinoline-3-carbaldehyde in good yield (see Table 1). The complexes were then synthesized in 1:2 metal:ligand [**M:HL**] ratio with metal salts of zinc chloride and cobalt chloride hexahydrate. The physicochemical properties of the ligand and metal complexes are summarized in Table 1.

3.1.1. Preparation of the Ligand from Different Organic Compounds. A. Synthesis of Acetanilide from Fluoroaniline. A mixture of acetic anhydride and acetic acid was poured into aniline containing zinc dust and then refluxed (80 °C, 2 h), and TLC was used to monitor the reaction progress. After refluxing, the reaction mixture was poured into ice-cold water and then filtered using section filtration to obtain the product in the form of a white powder (Scheme 1).

B. Preparation of the Reagent (Vilsmeier reagent). The reagent (Vilsmeier reagent) was prepared based on reported studies.[2] Accordingly, Vilsmeier reagent was prepared from *N*,*N*-dimethylformamide and phosphoryl chloride. The two reactants were reacted for 30 min in an ice water bath in the presence of $CaCl_2$ in a reaction hood as shown in Scheme 2.

C. Reaction of Acetanilide and the Targeted Reagent. 2-Chloro-6-fluoroquinoline-3-carbaldehyde was prepared from acetanilide and Vilsmeier reagent, which was refluxed at 100 °C for 22 h in an oil bath. Then, the resultant mixture was poured in ice-cold water and then filtered using suction filtration to obtain a yellowish powder product (Scheme 3).

Recrystallization of the crude product was accomplished using ethyl acetate at its boiling point, which afforded good crystals with very good yield. Derivatization of the product was accomplished using ethanolamine with the recrystallized product by worming for 2 h at 80 °C in an oil bath. Then, after completion of the reaction, the mixture product was poured into ice-cold water and filtered using suction filtration (Scheme 4).

The ligand $\mathbf{H_2L}$ [(*E*)-2-(((6-fluoro-2-((2-hydroxyethyl)-amino)quinolin-3-yl)methylene)amino)ethanol] is soluble in polar solvent, has a melting point of 65−70 °C, yield 87%, and is yellow in color. The analysis using different spectroscopies showed ^{1}H NMR (400 MHz, DMSO) δ 9.49 (1H, s, H-4), 8.48 (1H, d, J = 8.6 Hz, H-8), 8.18 (1H, t, J = 2.3 Hz, H-9), 7.52 (2H, H-5(d) and H-7(dd), J = 8.9 Hz), 4.88 (1H, t, J = 7.5 Hz, H-14), 4.73 (2H, td, J = 9.4 Hz, H-16), 3.68 (2H, td, J = 9.4 Hz, H-12), 3.41 (2H, td, J = 9.2 Hz H-15), 2.50 (2H, s, H-13 and 17); ^{13}C NMR (101 MHz, DMSO) δ 163.6 (C-2), 158.3 (C-9), 155.0 (C-6), 145.3 (C-8a), 142.2 (C-4), 127.8 (C-8), 122.2 (C-4a), 122.1 (C-3), 120.6 (C-7), 111.9 (C-5), 63.6 (C-11), 61.2 (C-16), 60.3 (C-12), 43.4 (C-15) (Figure S1 and S2). Elemental analysis: Calc. for $C_{14}H_{16}FN_3O_2$: C, 60.64; H, 5.82; F, 6.85; N, 15.15; and O, 11.54. Found C, 60.46; H, 5.60; F, 6.53; N, 14.95; O, 11.33.

3.1.2. Preparation of Complexes. The schematic representation for the synthesis of the complexes is presented in Scheme 5.

Complex **1** has the molecular formula $[Zn(HL)_2]$; light yellow powder; yield: 68%; melting point: 205−210 °C; soluble

https://doi.org/10.1021/acsomega.4c05560
ACS Omega 2024, 9, 36761−36777

Scheme 5. Proposed Chemical Synthesis of $[Zn(HL)_2]$ and $[Co(HL)_2(H_2O)_2]$ of Ligand H_2L [H_2L = (*E*)-2-(((6-fluoro-2-((2-hydroxyethyl)amino)quinolin-3-yl)methylene)amino)ethanol]

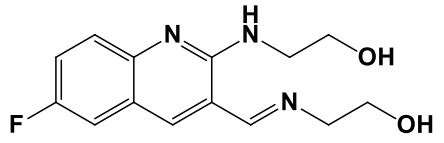

(*E*)-2-(((6-fluoro-2-((2-hydroxyethyl)amino)quinolin-3-yl)methylene)amino)ethanol

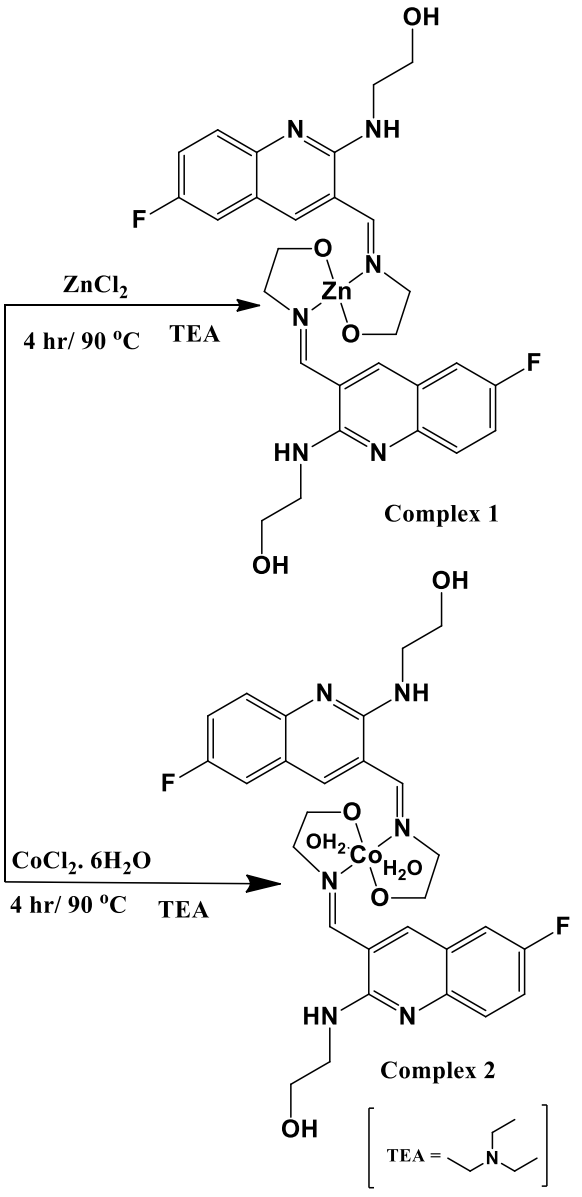

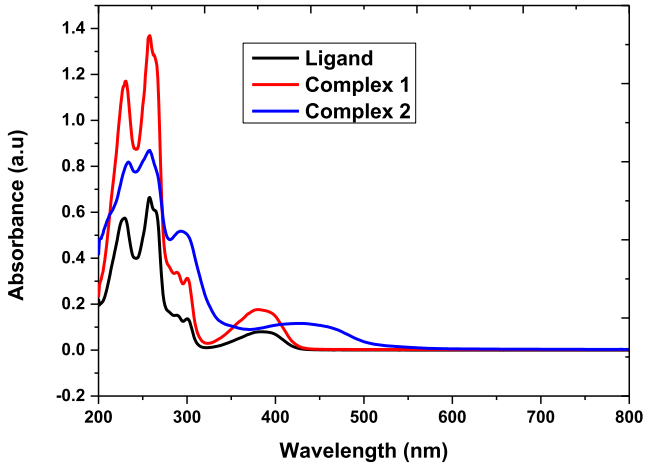

Figure 2. UV−vis spectra of the ligand and the complexes.

in polar solvents. Molar conductance (MeOH): 8.30 ± 0.31 Ω^{-1} mol^{-1} cm^2 at 25 °C. Elemental analysis, Calc. for $C_{28}H_{30}F_2N_6O_4Zn$: C, 54.42; H, 4.89; F, 6.15; N, 13.60; O, 10.36; Zn, 10.58%. Found C, 54.15; H, 4.68; F, 5.95; N, 13.33; O, 10.17; and Zn, 10.35%. FTIR (υ cm^{-1}, KBr (pellet)): 1659 ν(Imin C═N), 1037 ν(C−O), 528 ν(Zn−O), 457 ν(Zn−N), $[M^+ + H]$ at m/z = 616.90 (617.04).

Complex **2** has the molecular formula $[Co(HL)_2(H_2O)_2]$; deep brownish powder; yield: 65%; melting point: 255−260 °C; soluble in polar solvents. Molar conductance: 10.36 ± 0.42 Ω^{-1} $mol^{-1}cm^2$ at 25 °C. Elemental analysis, Calc. for $C_{28}H_{34}CoF_2N_6O_6$: C, 51.94; H, 5.29; Co, 9.10; F, 5.87; N, 12.98, and O, 14.82%. Found C, 51.82; H, 5.11; Co, 8.83; F, 5.62; N, 12.72; and O, 14.57%. FTIR (υ cm^{-1}, KBr (pellet)): 1652 ν(Imin C═N), 1059 ν(C−O), 543 ν(Co−O), 460 ν(Co−N), $[M^+ + H]$ at m/z = 647.30 (647.54).

3.2. Characterization of the Ligand and Its Zn(II) and Co(II) Complexes. *3.2.1. UV−Visible Spectroscopy.* The electronic spectra of both the ligand and its Zn(II) and Co(II)

https://doi.org/10.1021/acsomega.4c05560
ACS Omega 2024, 9, 36761−36777

Table 2. Selected FTIR Vibrations and Band Assignments for the Ligand and Its Complexes[a]

compounds	ν(O−H)	ν(N−H)	Im. ν(C═N)	Ql. ν(C═N)	ν(C−O)	ν(M−O)	ν(M−N)
Ligand	3374^{m} (3747, 3746)	3280^{m} (3536)	1640^{s} (1674)	1619^{s} (1610)	1054^{m} (1046,1038)	-	-
Complex **1**	3352^{w} (3753, 3751)	3011^{w} (3450, 3201)^{w}	1659^{s} (1690, 1657)	1634^{s} (1618, 1612)	1037^{m} (1100,1099)	528^{m} (521,500)	457^{m} (391)
Complex **2**	3663−3330^{b,w} (3750) (3652)	3191^{w} (3551−3323)	1652^{s} (1664−1654)	1630^{s} (1569−1552)	1059^{s} (1078, 1038, 1035)	543^{w} (559)	460^{w} (523)

[a]Experimental results are without parentheses, whereas the B3LYP-GD3/6-311++G**/LanL2DZ-calculated results are presented in parentheses. S = strong, m = medium, b = broad, w= weak—needs discussion based on metal d-electrons.

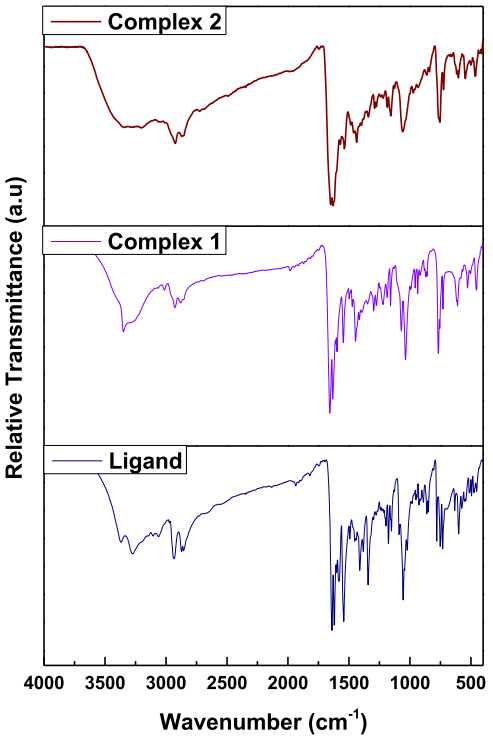

Figure 3. FTIR spectra of a ligand and its metal complexes.

complexes were recorded at wavelength range (200−800 nm) using a 1×10^{-5} M methanolic solution of the samples at room temperature and the results are presented in Figure 2. The UV−vis absorption spectra are produced possibly due to the electronic transitions from the highest occupied molecular orbital (HOMO) to the lowest unoccupied molecular orbital (LUMO).[33] The obtained spectra showed ligand bands due to ($\pi \rightarrow \pi^*$) and ($n \rightarrow \pi^*$) transitions, which undergo red and blue shifts under metal complexation. The bathochromic and hypsochromic shifts observed confirmed the formation of the targeted metal complexes.[33]

The free ligand absorption bands were recorded from the lowest to the highest wavelength (Figure 2), representing $\pi \rightarrow \pi^*$ (C═N) and $n \rightarrow \pi^*$ (C−O) electronic transitions, respectively. However, in the case of the Co(II) complex as compared to the Zn(II) complex, these bands exhibit bathochromic (red) shift at different absorbance due to the dominance of interligand electron transfer since zinc has a d^{10} electron configuration.[26] The Co(II) complexes' characteristic spectra were observed in different wavelength ranges, which would be assigned to the $\pi \rightarrow \pi^*$ and $n \rightarrow \pi^*$ transitions, respectively.[50] But, the broad bands observed at a higher wavelength were mainly due to the ligand to metal charge transfer (LMCT), which is in line with the previously reported studies;[23,32,51−56] hence, the ligand might have participated in the metal complex and this is because the ligand has a lone pair of electrons and the metals have vacant d-orbitals.[50] The TD-DFT calculation was obtained from the optimized geometries of the targeted complexes (Figure 1) and the corresponding theoretical peaks were in very good agreement with the experimental results (Figure S3).

3.2.2. Fluorescence Spectroscopy. The fluorescence spectra of both the ligand and its metal complexes were recorded in methanol within the wavelength range of 350−750 nm at room temperature using 10^{-5} M concentration of both the free ligand and its metal complexes.[57,58]

The emission spectra of the ligand and its complexes (**1** and **2**) showed emission bands at 526, 608, and 521 nm, respectively

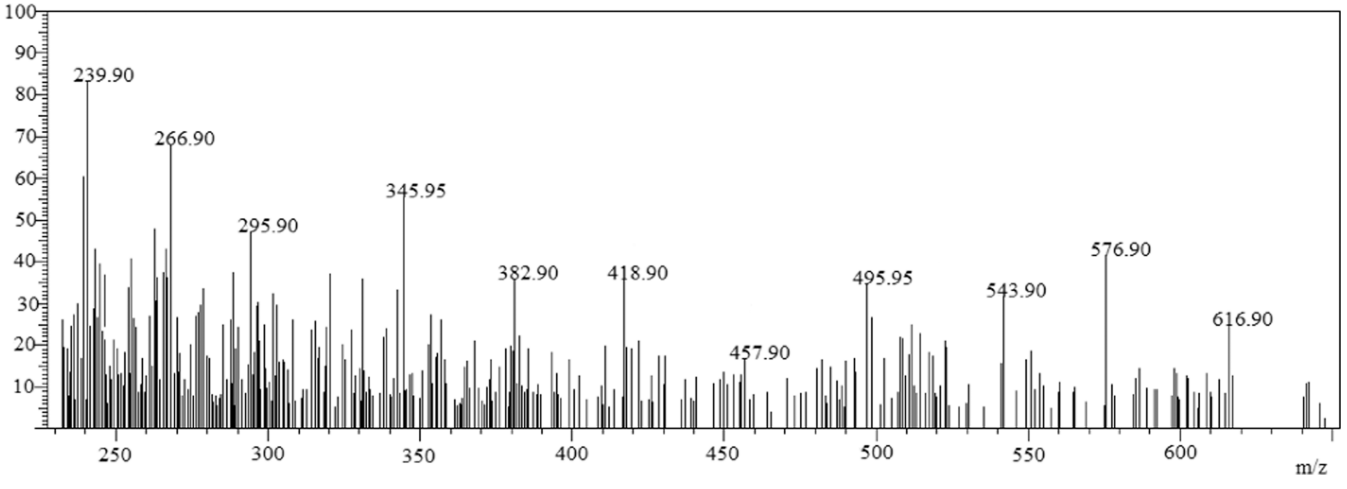

Figure 4. Mass spectra of complex **1**.

https://doi.org/10.1021/acsomega.4c05560
ACS Omega 2024, 9, 36761−36777

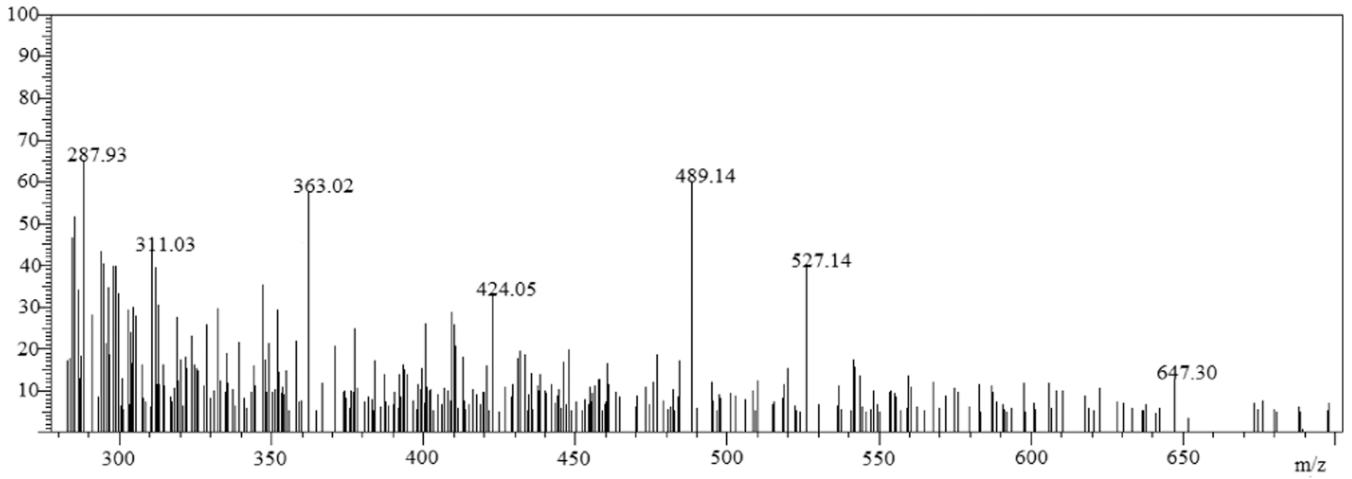

Figure 5. Mass spectra of complex **2**.

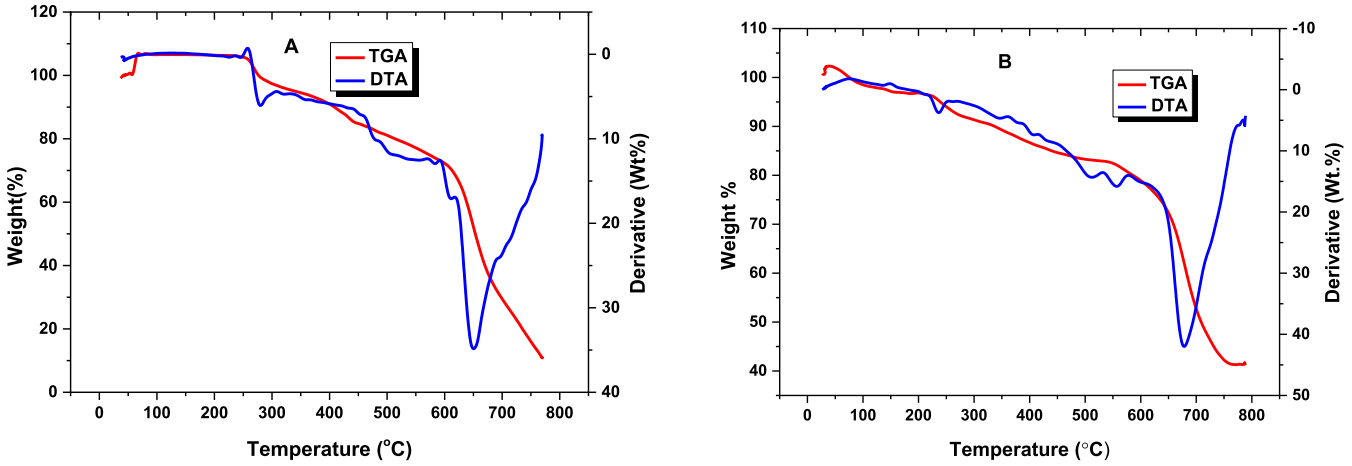

Figure 6. TGA and DTA curves of (A) complex **1** and (B) complex **2**.

Table 3. Temperature Range and Weight Loss Values for the Complexes[a]

			mass loss (%)		
compounds	decom. temp (°C)	DTA_{max} (°C)	obsd	calcd	interpretation
complex **1**	257−450	282	19.57	19.64	loss due to C_2H_6NO + C_2H_6NO-like moieties
	450−475	458	6.1	6.15	loss of two fluorine atoms
	475−665	649	40.78	40.83	loss of $C_9H_4N_3$ + $C_9H_4N_3$ species of the quinoline ring moieties
	665−750	693	17.80	17.90	loss of C_3H_5N + C_3H_5N moieties
complex **2**	219−245	234	5.56	5.60	loss of two water molecules
	250−530	510	18.54	18.90	loss of two C_2H_6NO + C_2H_6NO moieties
	530−655	559	5.90	5.93	loss of two species of fluorine atoms
	655−750	679	38.92	38.94	loss of C_9H_4N + C_9H_4N moieties
	750−787	765	16.98	17.03	loss of C_3H_5N + C_3H_5N moieties

[a]Decom. Temp = decomposition temperature, Obsd = observed, Calcd = calculated.

(Figures S4 and S5). The fluorescent intensity changes were observed after complexation, which is in agreement with the literature reports.[28] This corroborates the fact that coordinating with metal ions might make the ligand more rigid, as coordination complexes transfer energy from the excited state of the ligand to the metal ions. This resulted in fluorescence intensity shifts of the complexes, demonstrating that the material may be suitable for photochemical applications.[28,59,60]

The photoluminescence properties of zinc complexes are typically caused by intraligand emissions because of the d^{10} electron configuration; as a result, the complexes' luminescence is primarily caused by the coordination of the ligand to Zn(II) and is consistent with recently published studies.[59,61,62] In the case of Co(II), it exhibits altered emission intensities relative to the free ligand due to charge transfer, which is in agreement with reported studies.[9,10] Generally, the emission intensities showed hyperchromic/hypochromic and bathochromic/hypsochromic shifts upon complexation, and this indicates that the ligand fully participated in coordinate covalent bond formation, in which the

https://doi.org/10.1021/acsomega.4c05560
ACS Omega 2024, 9, 36761−36777

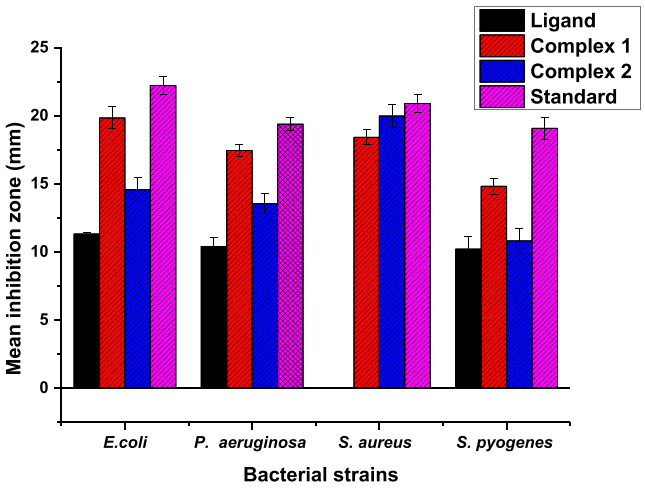

Figure 7. Mean inhibition zone of the antibacterial activity of the ligand and the complexes (n = 3). Error bars indicate standard deviation.

Table 4. MIC Values of the Complexes against Four Bacterial Strains in μg/mL

	complexes and standard		
bacterial strains	complex **1**	complex **2**	ciprofloxacin
E. coli	0.20	6.40	<0.025
P. aeruginosa	3.2	6.04	0.40
S. aureus	3.2	2.4	0.40
S. pyogenes	6.4	12.8	3.2

emission peaks of the complexes have been blue-shifted (Figure S3), which is in very good agreement with a reported study.[59]

3.2.3. FTIR Spectroscopy. The FTIR spectra of the free ligand and of the metal complexes were recorded using a 10 mg sample with KBr pellets in the wavenumber range of 4000−400 cm^{-1}, for which the detailed explanation is shown in Table 2 and Figure 3. The results of IR data were studied comparatively with theoretical vibrational IR data, which represent experimental/theoretical data. The IR spectrum of the ligand shows a stretching band at 1640/1674 cm^{-1} for the ν(C═N) imine group, but this band shifted toward different frequencies in the spectra of both metal complexes (**1** and **2**) to the range 1652−1659/1654−1690 cm^{-1}, indicating the participation of the nitrogen atom of the imine group ν(C═N) in coordinate covalent bonds (Table 2), which is in very good agreement with the reported studies.[10,33,41] In other case, the FTIR stretching frequency of the ligand at 3374/3746 cm^{-1} ν(O−H) is decreased in the case of all complexes, and this also shows the deprotonation of the hydroxyl group and participation of oxygen in the dative bond formation of complexation. In addition, the FTIR stretching frequency of the ligand at 3280/3536 cm^{-1}, ν(N−H), is decreased in the case of the synthesized metal

Table 6. Minimum Binding Energy and Interacting Amino Acids in the Molecular Docking of Complexes and Ligand and against *E. coli DNA Gyrase* (PDB ID: 6f86)

			residual interactions	
compounds	binding energy (kcal/mol)	H-bond	hydrophobic/Pi−sigma/anion	van der Waals
complex **1**	−7.2	Asn-46, Glu-50, Gly-77	Gly-77, Ile-94, Glu-50, Ile-78, Ile-94	Ala-47
complex **2**	−7.0	Gly-77	Asn-46, Asp-73, Ile-78, Pro-79	Ala-47
ligand	−6.2	Glu-50, Asn-46, asp-73	Ile-78. Ile-94	
ciprofloxacin	−7.3	Asp-46, Arg-76	Glu-50, Gly-77, Ile-78, Ile-94	

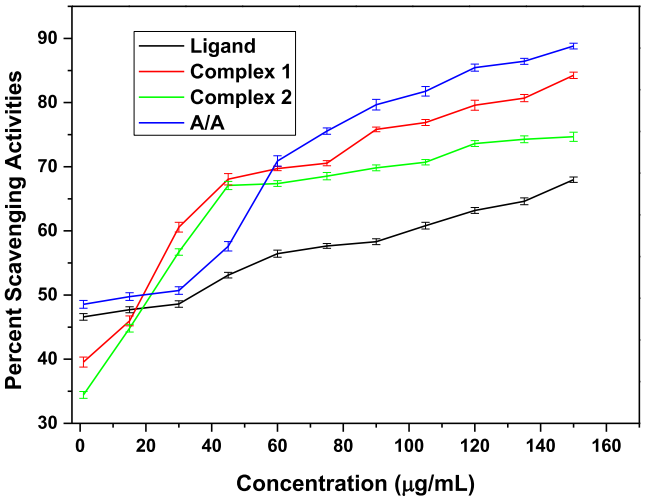

Figure 8. Percentage of free radical scavenging activities of the ligand and its complexes and ascorbic acid.

complexes, which indicates that there is no participation of nitrogen of the amine group in complex formation.

The weak and broad band stretching frequencies, which are in the range 3666−3330 cm^{-1}, could be assigned to the stretching vibration of water molecules that act as the water of coordination for the Co(II) complex. In addition, new stretching vibration bands were displayed at 528/521 cm^{-1} ν(Zn−O), 457/391 cm^{-1} ν(Zn−N), 543/559 cm^{-1} ν(Co−O), and 460/523 cm^{-1} ν(Co−N) bonds for Zn(II) and Co(II) complexes, respectively (Table 2). These show that metal ions participated in the coordinate covalent bond formation process.[10,33,41,63]

In addition, the presence of a weak bending vibration of δ(O−H) was observed in the range of 1470−1381 cm^{-1} in both metal complexes, confirming the appearance of the free bending hydroxyl (O−H) group as reported elsewhere in previous studies.[19,33] The DFT-calculated IR frequencies and TD-DFT-

Table 5. HOMO, LUMO, Energy Gap (E_g), Chemical Potential (μ), Hardness (η), Softness (σ), Electrophilicity (ω), Nucleophilicity Index (Nu), and Dipole Moment of the Compounds[a]

cpds.	HOMO	LUMO	E_g (eV)	μ	η	σ	ω	Nu	dipole M
H_2L	−8.310	−5.523	2.787	6.916	1.393	0.359	17.168	0.058	4.192
1	−6.486	−5.483	1.003	5.984	0.501	0.997	35.714	0.028	7.45
2	−6.522	−5.907	0.614	6.215	0.307	1.627	62.857	0.016	5.166

[a]Note: 1 = Complex **1**; 2 = Complex **2**

https://doi.org/10.1021/acsomega.4c05560
ACS Omega 2024, 9, 36761−36777

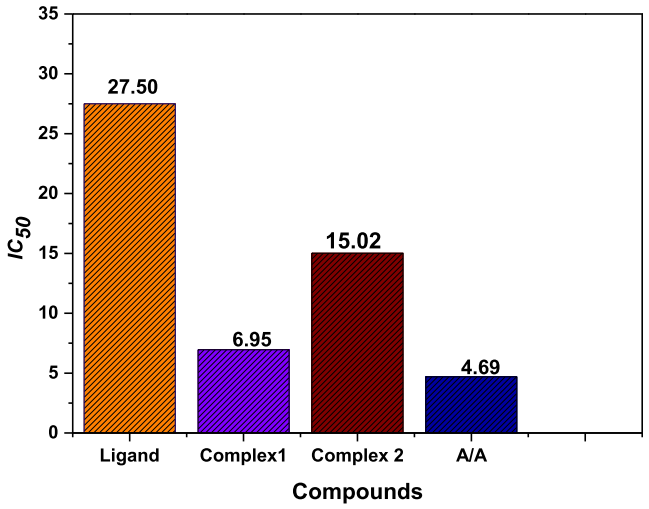

Figure 9. IC_{50} of the ligand and its complexes and ascorbic acid.

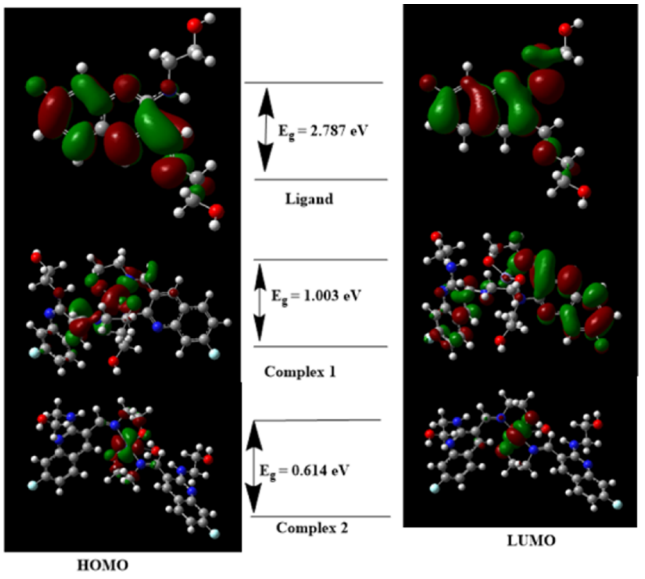

Figure 10. HOMO and LUMO of the ligand and its complexes (DFT/B3LYP/6-311++Gdp).

calculated absorption spectra were also in good agreement with the corresponding experimental results (Table 2), which further confirmed the successful synthesis of the targeted compounds.

3.2.4. Mass Spectra of Transition Metal Complexes. The mass spectra of the newly synthesized complexes (**1** and **2**) were recorded using LC-MS. Accordingly, the mass spectrum of complex **1** exhibited a parent molecular ion peak $[M^+ + H]$ at m/z = 616.90 (found = 617.04), which corresponds to the formula $[C_{28}H_{30}F_2N_6O_4Zn]$ (M.Wt. = 617.95 g/mol). The mass spectra of this complex displayed other peaks at m/z 495.95 (35.70%) (found = 496.80), 457.90 (15.75%) (found = 458.81), and 382.90 (39.75%) (found = 383.72), assignable to the $[C_{24}H_{18}F_2N_4O_2Zn]^+$, $[C_{24}H_{18}N_4O_2Zn]^+$, and $[C_{18}H_{15}N_4O_2Zn]^+$ fragments, respectively (Figure 4). Complex **2** exhibited a parent molecular ion peak at m/z = 647.30 (found= 647.54), which corresponds to the formula $[C_{28}H_{34}CoF_2N_6O_6]$ (M.Wt. = 647.54 g/mol). In addition, this complex showed other peaks at m/z = 527.14 (40.70%) (found = 527.39), 489.14 (60.75%) (found = 489.39), 363.02 (59.75%) (found = 363.25), and 287.93 (65.75%) (found = 288.17), which could be assigned to $[C_{24}H_{22}CoF_2N4O_4]^+$, $[C_{24}H_{22}CoN_4O_4]^+$, $[C_{15}H_{18}CoN_3O_4]^+$, and $[C_9H_{15}CoN_3O_4]^+$ fragments, respectively (Figure 5). This analysis is in agreement with the reported studies.[24,64,65]

3.2.5. Thermogravimetric Analysis. Thermogravimetric analysis (TGA) and differential thermal analysis (DTA) of the synthesized Zn(II) and Co(II) complexes (**1** and **2**) were carried out under N_2-atmosphere (20 mL/min) using 10 mg of the dried samples to get information about their thermal stability and to suggest a general scheme for their thermal decomposition as well as to ensure the presence and absence of water molecules. The TGA and DTA curves for the complexes (**1** and **2**) are presented in Figure 6, whereas the temperature range values for decomposition along with the corresponding weight loss values for each step of the decomposition reaction are presented in Table 3.

Accordingly, the TGA diagram of complex **1** $[C_{28}H_{30}F_2N_6O_4Zn]$ showed four decomposition stages (Figure 6A). The first degradation was observed in the temperature range of 257−450 °C (DTA_{max} = 282 °C), which indicates a mass loss of 19.57% (calcd. = 19.64%) attributed to the loss due to C_2H_6NO + C_2H_6NO-like moieties. The complex is stable up to 250 °C, which implies the absence of both lattice and the coordination water in the specified complex.[33,66] The second

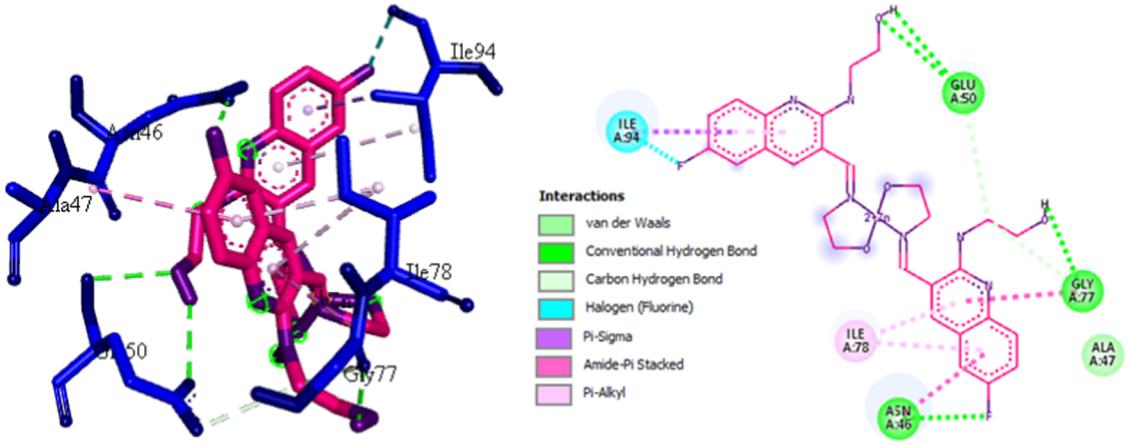

Figure 11. Binding interactions of complex **1** against *E. coli* DNA gyrase B (PDB ID: 6F86).

https://doi.org/10.1021/acsomega.4c05560
ACS Omega 2024, 9, 36761−36777

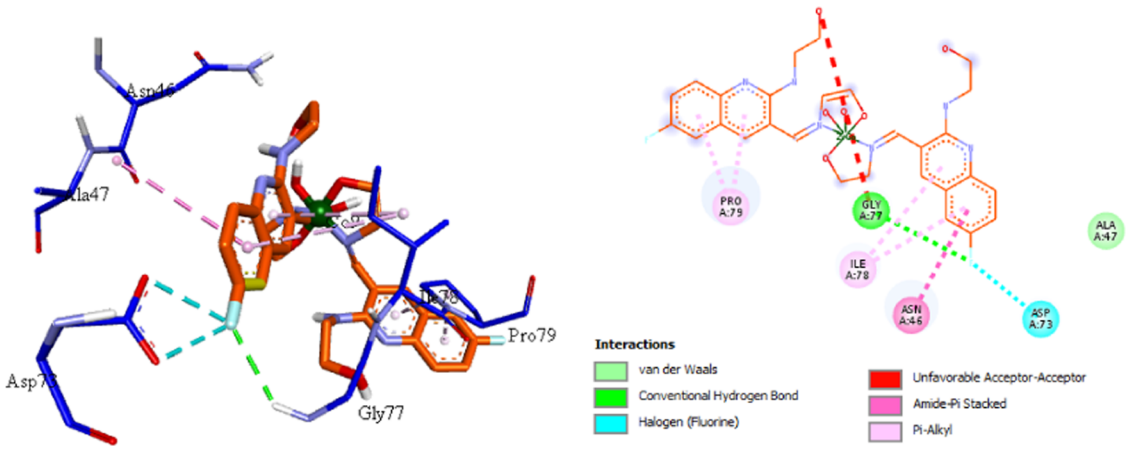

Figure 12. 3D and 2D binding interactions of complex **2** against *E. coli* DNA gyrase B (PDB ID: 6F86).

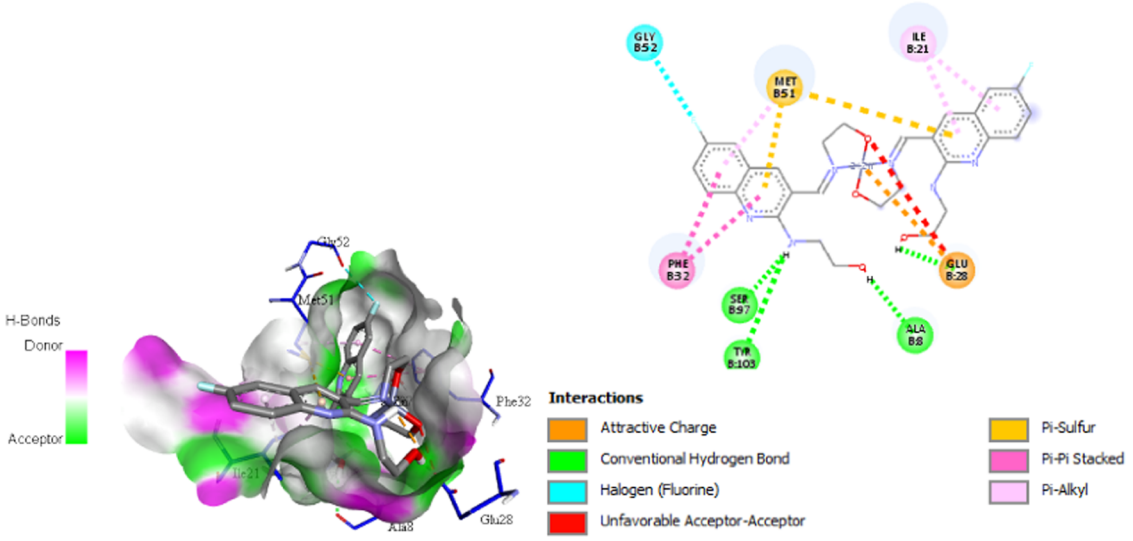

Figure 13. 3D and 2D binding interactions of complex **1** against against *E. coli* against *dihydrofolate reductase B* (7r6g) (PDB ID 5fsa).

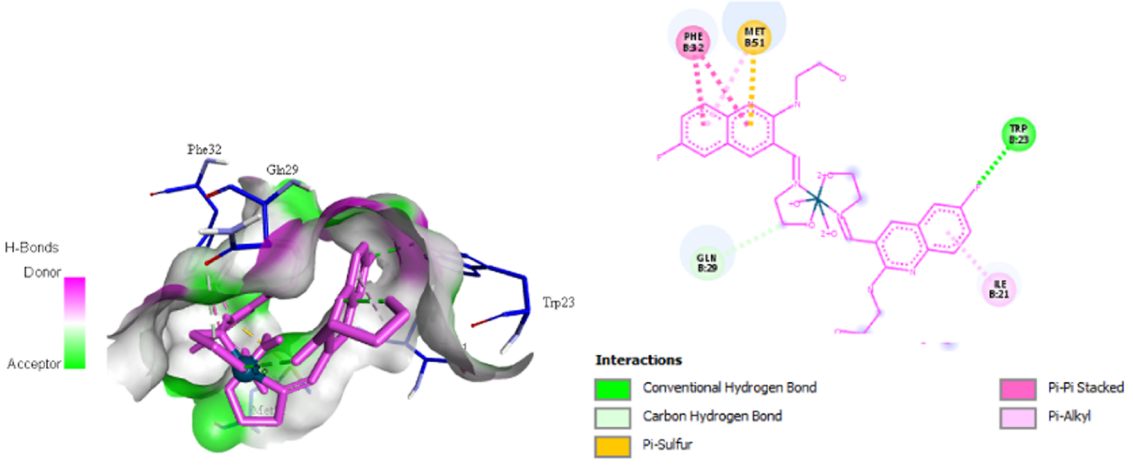

Figure 14. 3D and 2D binding interactions of complex **2** against *E. coli* against *dihydrofolate reductase B* (7r6g) (PDB ID 5fsa).

stage observed with a weight loss of 6.1% (calcd. = 6.15%) is attributed to the loss due to two fluorine atom moieties at 450−475 °C (DTA_{max} = 458 °C). The third stage of degradation arose from the mass loss of 40.78% (calcd. = 40.83%), attributed to the loss due to the $C_9H_4N_3$ + $C_9H_4N_3$ species of the quinoline ring moiety in the temperature range of 475−665 °C (DTA_{max} = 649 °C). The fourth and final step of degradation occurs in the temperature range of 665−750 °C with a weight loss of 17.8% (calcd. = 17.9%), attributed to the loss of C_3H_5N + C_3H_5N moieties. The actual weight loss that occurred from all of these

https://doi.org/10.1021/acsomega.4c05560
ACS Omega 2024, 9, 36761−36777

Table 7. Minimum Binding Energy and Interacting Amino Acids in the Molecular Docking of Complexes and Ligands and against *S. aureus tyrosyl-tRNA synthetase* (PDB ID: 1JIJ)

compounds	binding energy (kcal/mol)	H-bond	hydrophobic/Pi–sigma/anion
complex **1**	−8.0	Asp-40, Lys-84, Arg-88, Tyr-170, Gly-193, Gln-196, Asp-199	Cys-37, Ala-39, His-50, pro-58, Asp-80, Spn-80,
complex **2**	−10.5	Tyr-170, His-30	His-50, Pro-53, Asp-80, Gln-190, Asp-195, Pro-222
ligand	−8.0	Asp-40, Asp-80, Gln-174, Gly-193, Asp-195, Gln-196	Lue-70, Asp-177
SB-239629 (ref)	−8.1	Asp-40, His-50, Asp-80, Lys-84, Arg-88, Glu-190, Asp-195	Lys-37

steps is 84.25%, which is in very good agreement with the calculated value (84.52%).[66] Hence, gradual degradation was observed up to 750 °C and the residue corresponding to zinc oxide (ZnO) of about 15.75% (calcd = 15.48%) weight was recorded.[65,66]

The TGA diagram of complex **2**, $[C_{28}H_{34}CoF_2N_6O_6]$, exhibited five degradation stages (Figure 6B). The first stage of decomposition occurred in the temperature range of 219–245 °C (DTA_{max} = 234 °C), which corresponds to a mass loss of 5.56% (calcd = 5.60%) due to the loss of two water molecules. The second stage of decomposition occurred in the temperature range of 250–530 °C (DTA_{max} = 510 °C), which is accompanied by a weight loss of 18.544% (calcd. = 18.90%) corresponding to the loss of two C_2H_6NO + C_2H_6NO moieties. The third stage of degradation occurred in the temperature range of 530–655 °C (DTA_{max} = 559 °C) and was accompanied by a weight loss of 5.90% (calcd = 5.93%) corresponding to the loss of two species of fluorine atoms. The fourth stage arises due to a weight loss of 38.917% (calcd. = 38.94%) in the temperature range of 655–750 °C (DTA_{max} = 679 °C), corresponding to the elimination of C_9H_4N + C_9H_4N-like moieties. The fifth and final stage occurs in the temperature range of 750–787 °C (DTA_{max} = 765 °C), due to the loss of 16.983% (calcd. = 17.03%) related to C_3H_5N + C_3H_5N moieties, leaving behind a residue of cobalt(II) oxide (CoO), and the actual weight loss is 85.904%, which is very close to the calculated one (86.4%), in line with reported studies.[65,66]

The general degradation pattern of the complexes (**1** and **2**) had four and five stages, respectively, and the thermograms above 750 and 787 °C for complexes **1** and **2**, respectively, gave a straight line, indicating the formation of metal oxides.[67] The obtained percentage contents of elements in these complexes from both the elemental and TGA analyses are in line with the formulas proposed from the analytical data (see Section 3), and the thermogram of the complexes showed that the complexes are stable up to 100 °C with no weight loss observed below this temperature.

3.2.6. Molar Conductance. The molar conductance of the newly synthesized compounds was recorded in triplicate using methanol at a concentration of 1 mM at room temperature. The molar conductance of metal complexes (**1** and **2**) ranged from 8 to 11 Ω^{-1} mol^{-1} cm^2 at 25 °C (Table 1). These indicate that the conductivity of the synthesized metal complexes was relatively low, attributed to the nonelectrolytic nature of the complexes. This is mainly due to the fact that the metal cations received electrons from the ligand to make the net charge balance of the complexes zero, in line with the previous reported studies.[24] The absence of chloride ions was confirmed by the absence of a white precipitate during the chloride test performed using silver nitrate ($AgNO_3$). Therefore, the synthesized Zn(II) and Co(II) complexes were formulated as $[Zn(HL)_2]$ and $[Co(HL)_2(H_2O)_2]$, which is in agreement with the DFT-calculated results and reported studies.[16,32]

3.3. Biological Application. *3.3.1. Antibacterial Activities of the Ligand and Its Metal Complexes.* The *in vitro* antimicrobial activities of the compounds were tested against two Gram-negative (*E. coli* and *P. aeruginosa*) and two Gram-positive (*S. aureus* and *S. pyogenes*) human pathogenic bacterial strains (Table S1 and Figure 7).

The synthesized complexes were proven to have a range of activities against the targeted bacterial strains, with the mean zones of inhibition for the complexes ranging from the lowest (11 mm) to the highest (20 mm at 200 g/mL). Complex **1** showed very good activities against *E. coli* with mean inhibition zones of 19.84 ± 0.81 mm compared with the positive standard that showed maximum mean inhibition zones of 22.22 ± 0.66 mm at the same concentration (200 μg/mL). The free ligand showed a lower mean inhibition zone for all bacterial strains considered under this study, thus confirming that when the metal is incorporated into the ligand, the biological activities of the ligand will be enhanced due to the synergetic effect, which is also in line with reported studies.[10,33,41]

Furthermore, the MIC results shown in Table 4 proved better antibacterial activity for complex **1** against *E. coli* and *P.*

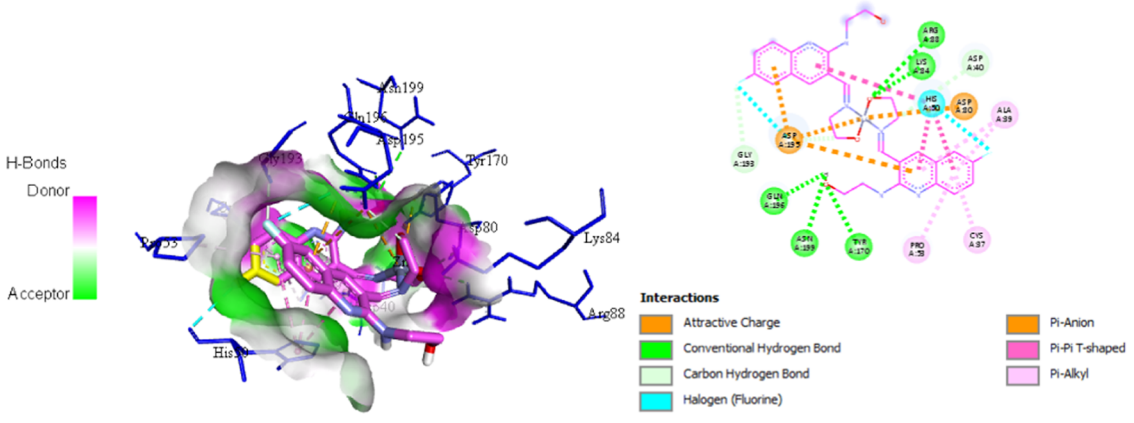

Figure 15. 3D and 2D binding interactions of complex **1** against *S. aureus tyrosyl-tRNA synthetase*.

https://doi.org/10.1021/acsomega.4c05560
ACS Omega 2024, 9, 36761–36777

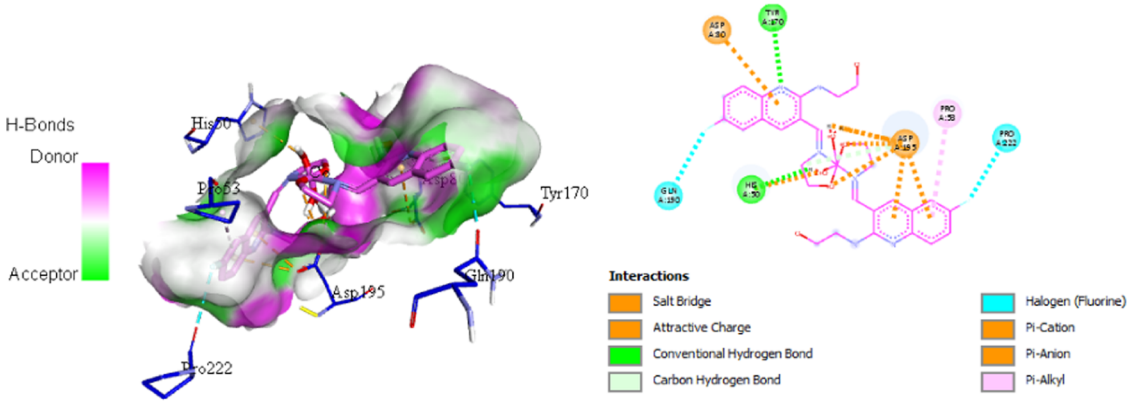

Figure 16. 3D and 2D binding interactions of complex **2** against *S. aureus tyrosyl-tRNA synthetase*.

aeruginosa, and for complex **2** against *S. aureus* with MIC values of 0.2, 3.2, and 2.4 (μg/mL), respectively. Therefore, metal complexes showed significant antibacterial activity against Gram-negative and Gram-positive bacteria with smaller MIC values.

The antibacterial results of the synthesized complexes showed much better activities than the ligand (Tables 4 and 5). Thus, the results of this experiment indicated that the addition of fluorine substituents in the quinoline ring might improve the bioactivity of the complexes further and lead to the development of new and effective antimicrobial agents.

In other ways, the higher percent activity indexes of the newly synthesized complex against all of the examined bacterial strains may be due to the borderline acid nature of both Zn(II) and Co(II) ions. This helps the complexes to easily bind with similar biomolecules such as protein and enzyme by the "hard soft acid−base (HSAB)" principle. Hence, the complex showed good binding activity with both G. negative and G. positive (*E. coli* and *S. aureus*) bacteria due to the H-bonding interaction with amino acid-like arginine, which have both acid and base ends (see Section 3.4, Tables 5 and 6). In addition to this, coordination compounds can be highly effective in treating microbial infections due to the redox activity of the ions that interact with the bacterial chromosome, which leads to a decrease in bacterial reproduction.[68] This might be due to the chelation of the metal with the ligand, which promotes the ability of the complexes to penetrate the cell membrane of the bacterial strains.[51,65,69] Hence, chelation enhances the delocalization of π−electrons, which results in an increase of lipophilicity of the complexes. Due to increase in lipophilicity, the permeation of the specified complexes could be enhanced, which leads to inhibition of the binding sites in the enzymes of microorganisms.[51,63,65,67,69] This may result in the disturbance of the respiration system of the cell and prevent the synthesis of the proteins, which ultimately leads to the disappearance of the binding sites in an enzyme of the microorganisms.

3.3.2. Antioxidant Activity of the Ligand and Its Metal Complexes. The antioxidant activities of the free ligand and its metal complexes were analyzed in terms of their proton-donating ability with UV−visible absorbance using the DPPH assay. This assay is widely used to assess the ability of compounds as scavengers of free radicals and evaluate the antioxidant activity of target-free ligands and their metal complexes. In this work, the radical scavenging activities of the synthesized ligand and both complexes were evaluated and the findings are shown in Figure 8 and Table S2. The data indicate that the synthesized complexes showed very good antioxidant activities, while complex **1** showed better antioxidant activity with very good percent scavenging activities and the complexes showed higher antioxidant activities than the corresponding free ligand (Figure 8). This might be due to synergetic effects; hence, the complexes have a strong potential to be useful as radical scavengers, which is in line with the reported studies.[20,69] From the IC_{50} values presented, complex **1** showed better scavenging activities (Figure 9), which has a direct correlation with the good antioxidant properties, in line with reported studies.[65,69,70]

It is also well known that zinc complexes are important for the formation and functioning of several enzymes and proteins, such as alcoholic dehydrogenase, carbonic anhydrase, and Cu/Zn superoxide dismutase, which are involved in the processes of respiration, energy metabolism, catalyzing superoxide breakdown, and DNA synthesis, and these are highly correlated with free radical scavenging activities. The high activity was probably due to the presence of the OH group in addition to the oxidation potential of the metal ion, in agreement with the reported study.[25]

3.4. *In Silico* Analysis of Ligand and Its Metal Complexes. *3.4.1. Quantum Chemical Analysis.* Transitional metals and their complexes have been investigated by using computational chemistry. However, the main problem associated with studying the calculations with these systems is the electron degeneracy, which is partially configured in d-orbitals. Over the years, several studies have been conducted to confirm the efficacy of various DFT approaches for investigating the chemical properties of transition metal complexes. Among various properties, mixed basis sets have been very promising in computational studies and cover a wide range of ligands and their metal complexes.[32]

The band gap energy (E_g) is correlated with various biological aspects like antibacterial, antioxidant, and DNA binding activities.[32,33,41] It has been reported that the band gap energy difference between the E_{HOMO} and E_{LUMO} is an important stability descriptor.[32,33,41] A decrease in the band gap energy upon coordination may be associated with the presence of LMCT.[32] The quantum chemical parameters of the ligand and its metal complexes are listed in Table 5. The highest occupied molecular orbital (HOMO) and lowest unoccupied molecular orbital (LUMO) analysis was performed to predict the reactivity and biological activities of the ligand and its complexes. The energy gaps ($E_g = E_{LUMO} - E_{HOMO}$) for possible electron transition were calculated to be 2.787, 1.003, and 0.614 eV for the ligand and its complexes (**1** and **2**), respectively. These

https://doi.org/10.1021/acsomega.4c05560
ACS Omega 2024, 9, 36761−36777

results predict good biological activities of the synthesized compounds.[32]

The wave function analysis of the ligand revealed that the electron density of the molecule circulates between the secondary imine substituent nitrogen and the quinoline ring imine from HOMO to LUMO and throughout the quinoline ring due to π-bond delocalization. The HOMO and LUMO of the ligand reside on the quinoline ring, confirming the presence of $\pi \rightarrow \pi^*$ electron transition (Figure 10). It is also observed that the electron densities of the HOMO reside on the amine part of the molecule and those of the LUMO reside on its imine part. This is due to the fact that the amine and imine parts of the ligand are in the same plane, making it suitable for coordination compound formation.[71]

The selected quantum chemical parameters were derived from E_{HOMO} and E_{LUMO} and used to evaluate the chemical reactivity and biological activities of the complexes. In other ways, the complexation between the metal ions and the ligand reduced the HOMO−LUMO energy gap, which can be considered as an indication for better biological activities.[32,33] Accordingly, from the band gap analyses, the metal complexes were predicted to have biological activities better than those of the free ligand, in good agreement with the experimental biological activities.

Based on the dipole moment of the newly synthesized compounds, complex **1** showed higher biological activities toward appropriate molecules, which can be discussed considering the hard−soft−acid−base principle, which supports the *in vitro* biological activities[32] (Tables 4 and 5, see Section 3.3.1). Hence, the biological activity of a compound increases with increasing intermediate softness and hardness.[32,33] Accordingly, the biological structures of enzymes, which are commonly intermediate soft, prefer to bind with intermediate soft complexes. Hence, complex **1** prefers to bind with biological molecules. In another way, the chemical potential (μ) measures the tendency of an electron to escape from equilibrium, and it has been reported that the chemical reactivity of a compound increases with decreasing chemical potential.

The electrophilicity index implies the ability of the complexes to accept electrons, while nucleophilicity index displays the ability to donate electrons.[32,33] In this aspect, complex **2** has a stronger electron-accepting potential than complex **1**, whereas the free ligand is a bigger electron donor, based on its electrophilicity index and nucleophilicity index value, respectively (Table 5).

From both experimental (elemental analysis, MS and TGA) and DFT analyses, it could be deduced that the ligand acts as an ON donor bidentate chelating agent. The analyses also indicated that complex **1** has a distorted tetrahedral geometrical (Figure 1) and complex **2** showed an octahedral structure, in line with previously reported studies.[33,59,72]

3.4.2. Molecular Docking Analysis. Bacterial DNA gyrase is a bacterial type II topoisomerase enzyme, which maintains the negative supercoiled state of the chromosome during replication and transcription. In *E. coli*, the appropriate level of supercoiling is important for regulation transcription, replication, repair, and recombination.[73] Dihydrofolate reductase (DHFR) is another essential enzyme needed to maintain bacterial growth.[74] It is a crucial enzyme for the survival of the Gram-negative bacterial strains.[75] First- and second-line drugs for the treatment of *Mycobacterium tuberculosis* based on DHFR pose a great threat to human health. Thus, it is very important to design a novel and safe inhibitor of DHFR.[74] Tyrosyl-tRNA synthetase is another alternative bacterial enzyme that is essential to translate the coded information into protein structures in nucleic acids and inhibitors of Tyrosyl-tRNA synthetases may be also another target to develop novel drugs to treat bacterial diseases in humans.[76]

Based on the above anticipation and the results of *in vitro* antibacterial activities, the novel complexes (**1** and **2**) were docked into the active sites of the above three enzymes, and the results were compared with those of standard drugs and inhibitors. In case of *E. coli DNA gyrase B*, the binding affinities of the complexes were comparable to that of ciprofloxacin (−7.3 kcal/mol) (Table 6, Figures 11, and 12), as the complex showed a comparable inhibitor of *E. coli DNA gyrase* to that of ciprofloxacin. For *E. coli* dihydrofolate reductase B, the binding affinities of complex **1** and **2** were −9.9 and −8.0 kcal/mol, respectively, wherea it was −7.3 kcal/mol for trimethoprim (Table S3, Figures 13 and 14). Thus, in reference to *E. coli dihydrofolate reductase* B, both complexes were stronger inhibitors of the enzyme than the standard drug (Trimethoprim). The same correlation holds true for *S. aureus tyrosyl-tRNA synthetase*. The binding affinities of the complexes (**1** and **2**) were −8.0 and −10.5 kcal/mol, respectively, while it was −8.1 kcal/mol for the standard inhibitor (SB-239629), indicating again that complex **2** was a stronger inhibitor than the standard ligand while complex **1** was as strong as the standard ligand (Table 7, Figures 15 and 16), which agrees with *in vitro* bacterial evaluation results (Tables S1 and 4).

4. CONCLUSIONS

Quinoline derivative ligands have been a successful scaffold to develop bioactive molecules. In the present work, novel Zn(II) and Co(II) complexes were successfully synthesized from a bidentate ON atom's donor ligand $\mathbf{H_2L}$ [($\mathbf{H_2L}$) = (*E*)-2-(((6-fluoro-2-((2-hydroxyethyl)amino)quinolin-3-yl)methylene)-amino)ethanol]. The compounds were characterized with physicochemical and spectroscopic methods, which are supported via DFT and TD-DFT calculations. The DFT-calculated IR frequencies and TD-B3LYP-calculated absorption spectra are in good agreement with the corresponding experimental results. From both experimental and DFT analyses, it was found that the ligand acts as an ON donor bidentate chelating agent; hence, complex **1** was proposed to have a tetrahedral structure and complex **2** to have an octahedral geometrical structure. The *in vitro* antibacterial activity analysis revealed that both complexes demonstrated strong inhibition against *E. coli* and *S. aureus* compared to the free ligand. The *in silico* molecular docking studies suggest that the complexes may play a role in therapeutic approaches in the search for pharmacological intervention and treatment of health problems. In general, the *in silico* studies, which were in accordance with the *in vitro* studies, provided useful complementary insight into the elucidation of the mechanism of action of the studied complexes at the molecular level and the interpretation of their biological activity in many diseases. In addition, these results may also prove pioneering for novel or reported complexes of selected metal ions with other heterocyclic quinoline derivatives as ligands and their transition metal complexes in order to be examined in the future for their potential antibacterial and antioxidant activities. In addition, the research is an active and ongoing project in our group, and hence we will consider noncommunicable diseases in the progress of our research work in the future.

https://doi.org/10.1021/acsomega.4c05560
ACS Omega 2024, 9, 36761−36777

■ ASSOCIATED CONTENT

Supporting Information

The Supporting Information is available free of charge at https://pubs.acs.org/doi/10.1021/acsomega.4c05560.

^{1}H NMR, ^{13}C NMR, DEPT-135, FTIR, TD-DFT, Fluorescence, mean inhibition zone, percentage radical scavenging activity, and molecular docking results (PDF)

■ AUTHOR INFORMATION

Corresponding Author

Tadewos Damena − *Department of Chemistry, Wachemo University, 667 Hossana, Ethiopia;* orcid.org/0000-0001-5345-002X; Email: tad.dam.keb2010@gmail.com

Authors

Tegene Desalegn − *Department of Applied Chemistry, Adama Science and Technology University, 1888 Adama, Ethiopia;* orcid.org/0000-0003-0239-8326

Sadhna Mathura − *School of Chemistry, University of the Witwatersrand, Johannesburg 2050, South Africa*

Alemayehu Getahun − *Department of Biology, Wachemo University, 667 Hossana, Ethiopia*

Dereje Bizuayehu − *Department of Chemistry, Wachemo University, 667 Hossana, Ethiopia*

Mamaru Bitew Alem − *Department of Physics, University of Pretoria, Hatfield 0028, South Africa; National Institute for Theoretical and Computational Sciences (NITheCS), Dimbaza 5600, South Africa;* orcid.org/0000-0002-1880-8572

Shiferaw Gadisa − *Department of Physics, Wachemo University, 667 Hossana, Ethiopia*

Digafie Zeleke − *Department of Chemistry, Salale University, 245 Fitche, Ethiopia;* orcid.org/0000-0002-8908-2967

Taye B. Demissie − *Department of Chemistry, University of Botswana, 00704 Gaborone, Botswana;* orcid.org/0000-0001-8735-4933

Complete contact information is available at: https://pubs.acs.org/10.1021/acsomega.4c05560

Author Contributions

T. Damena and D.Z. conducted the experiments; T. Damena, D.Z., T. Desalegn, A.G., S.G., M.B.A, and T.B.D. performed the data analysis; T. Damena, D.Z., T. Desalegn, S.M., A.G., S.G., and T.B.D. prepared the methodology; T. Damena and D.Z. wrote the original draft; and T. Damena, D.Z., T. Desalegn, S.M., A.G., S.G., D.B., M.B.A., and T.B.D. participated in reviewing and editing the paper.

Notes

The authors declare no competing financial interest.

■ ACKNOWLEDGMENTS

The authors would like to acknowledge Wachemo University, Adama Science, Technology University, and University of Botswana for the research facilities. Computational resources were supplied by the project "e-Infrastruktura CZ" (e-INFRA CZ ID:90140) supported by the Ministry of Education, Youth and Sports of the Czech Republic.

■ REFERENCES

(1) Pinz, M. P.; Reis, A. S.; de Oliveira, R. L.; Voss, G. T.; Vogt, A. G.; Sacramento, M. do.; Roehrs, J. A.; Alves, D.; Luchese, C.; Wilhelm, E. A. 7-Chloro-4-Phenylsulfonyl Quinoline, a New Antinociceptive and Anti-Inflammatory Molecule: Structural Improvement of a Quinoline Derivate with Pharmacological Activity. *Regul. Toxicol. Pharmacol.* **2017**, *90*, 72−77.

(2) Digafie, Z.; Melaku, Y.; Belay, Z.; Eswaramoorthy, R. Synthesis, Molecular Docking Analysis, and Evaluation of Antibacterial and Antioxidant Properties of Stilbenes and Pinacol of Quinolines. *Adv. Pharmacol. Pharm. Sci.* **2021**, *2021*, 1−17.

(3) Zeleke, D.; Eswaramoorthy, R.; Belay, Z.; Melaku, Y. Synthesis and Antibacterial, Antioxidant, and Molecular Docking Analysis of Some Novel Quinoline Derivatives. *J. Chem.* **2020**, *2020*, 1−16.

(4) Nainwal, L. M.; Tasneem, S.; Akhtar, W.; Verma, G.; Khan, M. F.; Parvez, S.; Shaquiquzzaman, M.; Akhter, M.; Alam, M. M. Green Recipes to Quinoline: A Review. *Eur. J. Med. Chem.* **2019**, *164*, 121−170.

(5) Murugavel, S.; Jacob Prasanna Stephen, C. S.; Subashini, R.; AnanthaKrishnan, D. Synthesis, Structural Elucidation, Antioxidant, CT-DNA Binding and Molecular Docking Studies of Novel Chloroquinoline Derivatives: Promising Antioxidant and Anti-Diabetic Agents. *J. Photochem. Photobiol., B* **2017**, *173* (March), 216−230.

(6) Cretton, S.; Breant, L.; Pourrez, L.; Ambuehl, C.; Marcourt, L.; Ebrahimi, S. N.; Hamburger, M.; Perozzo, R.; Karimou, S.; Kaiser, M.; et al. Antitrypanosomal Quinoline Alkaloids from the Roots of Waltheria Indica. *J. Nat. Prod.* **2014**, *77* (10), 2304−2311.

(7) Amer, A. M.; El-Eraky, W. I.; Mahgoub, S. Synthesis, Characterization and Antimicrobial Activity of Some Novel Quinoline Derivatives Bearing Pyrazole and Pyridine Moieties. *Egypt. J. Chem.* **2018**, *61*, 1−8.

(8) Chen, Z. F.; Qin, Q. P.; Qin, J. L.; Zhou, J.; Li, Y. L.; Li, N.; Liu, Y. C.; Liang, H. Water-Soluble Ruthenium(II) Complexes with Chiral 4-(2,3-Dihydroxypropyl)-Formamide Oxoaporphine (FOA): In Vitro and in Vivo Anticancer Activity by Stabilization of G-Quadruplex DNA, Inhibition of Telomerase Activity, and Induction of Tumor Cell Apoptosis. *J. Med. Chem.* **2015**, *58* (11), 4771−4789.

(9) Damena, T.; Alem, M. B.; Zeleke, D.; Desalegn, T.; Eswaramoorthy, R.; Demissie, T. B. Novel Zinc (II) and Copper (II) Complexes of 2 - ((2- Hydroxyethyl) Amino) Quinoline-3-Carbaldehyde for Antibacterial and Antioxidant Activities: A Combined Experimental, DFT, and Docking Studies. *ACS Omega* **2022**, *7* (2022), 26336−26352.

(10) Damena, T.; Alem, M. B.; Zeleke, D.; Demissie, T. B.; Desalegn, T. Synthesis and Computational Studies of Novel Cobalt(II) and Oxovanadium(IV) Complexes of Quinoline Carbaldehyde Derivative Ligand for Antibacterial and Antioxidant Applications. *J. Mol. Struct.* **2023**, *1280*, No. 134994.

(11) Artemjev, A. A.; Astafiev, A. A.; Vologzhanina, A. V.; Kubasov, A. S.; Burkin, G. M.; Novikov, A. S.; Kritchenkov, A. S.; Kirichuk, A. A.; Tskhovrebov, A. G. Triarylazoimidazole-ZnII, CdII, and HgII Complexes: Structures, Photophysics, and Antibacterial Properties. *Crystals*, **2022**, *12* (5). 680.

(12) Bondarenko, M. A.; Rakhmanova, M. I.; Plyusnin, P. E.; Abramov, P. A.; Novikov, A. S.; Rajakumar, K.; Sokolov, M. N.; Adonin, S. A. Heteroleptic Zn(II) 3,5-Diiodosalicylates: Structures, Luminescence and Features of Non-Covalent Interactions in Solid State. *Polyhedron*, **2021**, *194*. 114895.

(13) Romashev, N. F.; Abramov, P. A.; Bakaev, I. V.; Fomenko, I. S.; Samsonenko, D. G.; Novikov, A. S.; Tong, K. K. H.; Ahn, D.; Dorovatovskii, P. V.; Zubavichus, Y. V.; et al. Heteroleptic Pd(II) and Pt(II) Complexes with Redox-Active Ligands: Synthesis, Structure, and Multimodal Anticancer Mechanism. *Inorg. Chem.* **2022**, *61* (4), 2105−2118.

(14) Roy, S.; Mal, S.; Banik, R.; Das, S.; Dlháň, L'.; Titiš, J.; Boča, R.; Kirillov, A. M.; Novikov, A. S.; Hazendonk, P.; et al. Two Isostructural Complexes of Ni(Ii) and Zn(Ii) with Violurate and Pyridine: A Detailed Structural, Theoretical, Magnetic, and NMR Investigation. *CrystEngComm* **2023**, *25* (46), 6503−6511.

(15) El-Sonbati, A. Z.; Diab, M. A.; Morgan, S. M.; Abou-Dobara, M. I.; El-Ghettany, A. A. Synthesis, Characterization, Theoretical and Molecular Docking Studies of Mixed-Ligand Complexes of Cu(II),

https://doi.org/10.1021/acsomega.4c05560
ACS Omega 2024, 9, 36761−36777

Ni(II), Co(II), Mn(II), Cr(III), UO2(II) and Cd(II). *J. Mol. Struct.* **2020**, *1200*, No. 127065.
(16) Abumelha, H. M.; Alkhatib, F.; Alzahrani, S.; Abualnaja, M.; Alsaigh, S.; Alfaifi, M. Y.; Althagafi, I.; El-Metwaly, N. Synthesis and Characterization for Pharmaceutical Models from Co(II), Ni(II) and Cu(II)-Thiophene Complexes; Apoptosis, Various Theoretical Studies and Pharmacophore Modeling. *J. Mol. Liq.* **2021**, *328*, No. 115483.
(17) Zianna, A.; Geromichalos, G.; Psoma, E.; Kalogiannis, S.; Hatzidimitriou, A. G.; Psomas, G. Structure and in Vitro and in Silico Biological Activity of Zinc(II) Complexes with 3,5−Dichloro−Salicylaldehyde. *J. Inorg. Biochem.* **2022**, *229* (2022), No. 111727.
(18) Frei, A.; Ramu, S.; Lowe, G. J.; Dinh, H.; Semenec, L.; Elliott, A. G.; Zuegg, J.; Deckers, A.; Jung, N.; Bräse, S.; et al. Platinum Cyclooctadiene Complexes with Activity against Gram-Positive Bacteria. *ChemMedChem* **2021**, *16* (20), 3165−3171.
(19) Zou, B. Q.; Lu, X.; Qin, Q. P.; Bai, Y. X.; Zhang, Y.; Wang, M.; Liu, Y. C.; Chen, Z. F.; Liang, H. Three Novel Transition Metal Complexes of 6-Methyl-2-Oxo-Quinoline-3-Carbaldehyde Thiosemicarbazone: Synthesis, Crystal Structure, Cytotoxicity, and Mechanism of Action. *RSC Adv.* **2017**, *7* (29), 17923−17933.
(20) El-Gammal, O. A.; Mohamed, F. S.; Rezk, G. N.; El-Bindary, A. A. Synthesis, Characterization, Catalytic, DNA Binding and Antibacterial Activities of Co(II), Ni(II) and Cu(II) Complexes with New Schiff Base Ligand. *J. Mol. Liq.* **2021**, *326*, No. 115223.
(21) Abu-Dief, A. M.; El-Metwaly, N. M.; Alzahrani, S. O.; Alkhatib, F.; Abualnaja, M. M.; El-Dabea, T.; El-Remaily, M. A. E. A. A. A. Synthesis and Characterization of Fe(III), Pd(II) and Cu(II)-Thiazole Complexes; DFT, Pharmacophore Modeling, in-Vitro Assay and DNA Binding Studies. *J. Mol. Liq.* **2021**, *326*, No. 115277.
(22) Hamdani, H. E. L.; Amane, M. E. L. Preparation, Spectral, Antimicrobial Properties and Anticancer Molecular Docking Studies of New Metal Complexes [M(Caffeine) 4] (PF 6) 2; M = Fe(II), Co(II), Mn(II), Cd(II), Zn(II), Cu(II), Ni(II). *J. Mol. Struct.* **2019**, *1184*, 262−270.
(23) Elsayed, S. A.; Badr, H. E.; di Biase, A.; El-Hendawy, A. M. Synthesis, Characterization of Ruthenium(II), Nickel(II), Palladium-(II), and Platinum(II) Triphenylphosphine-Based Complexes Bearing an ONS-Donor Chelating Agent: Interaction with Biomolecules, Antioxidant, in Vitro Cytotoxic, Apoptotic Activity and Cell. *J. Inorg. Biochem.* **2021**, *223* (April), 1−19.
(24) El-Sonbati, A. Z.; Diab, M. A.; Morgan, S. M.; Abou-Dobara, M. I.; El-Ghettany, A. A. Synthesis, Characterization, Theoretical and Molecular Docking Studies of Mixed-Ligand Complexes of Cu(II), Ni(II), Co(II), Mn(II), Cr(III), UO2(II) and Cd(II). *J. Mol. Struct.* **2020**, *1200* (2020), No. 127065.
(25) Fetoh, A.; El-Gammal, O. A.; Abu El-Reash, G. M. Antioxidant and Antitumor Activities of Cr(III), Mn(II), Fe(III), Cd(II), Zn(II) and Hg(II) Complexes Containing a Carbohydrazone Ligand Ending by 4-Pyridyl Ring. *J. Mol. Struct.* **2018**, *1173*, 100−110.
(26) Ekennia, A. C.; Onwudiwe, D. C.; Olasunkanmi, L. O.; Osowole, A. A.; Ebenso, E. E. Synthesis, DFT Calculation, and Antimicrobial Studies of Novel Zn(II), Co(II), Cu(II), and Mn(II) Heteroleptic Complexes Containing Benzoylacetone and Dithiocarbamate. *Bioinorg. Chem. Appl.* **2015**, *2015*, 1−12.
(27) Zianna, A.; Geromichalou, E.; Geromichalos, G.; Fiotaki, A.; Hatzidimitriou, A. G.; Kalogiannis, S.; Psomas, G. Synthesis, Characterization and in Vitro and in Silico Biological Profile. *J. Inorg. Biochem.* **2022**, *226* (November2021), No. 111659.
(28) Mandewale, M. C.; Kokate, S.; Thorat, B.; Sawant, S.; Yamgar, R. Zinc Complexes of Hydrazone Derivatives Bearing 3,4-Dihydroquinolin-2(1H)-One Nucleus as New Anti-Tubercular Agents. *Arab. J. Chem.* **2019**, *12* (8), 4479−4489.
(29) Fekadu, M.; Zeleke, D.; Abdi, B.; Guttula, A.; Eswaramoorthy, R.; Melaku, Y. Synthesis, in Silico Molecular Docking Analysis, Pharmacokinetic Properties and Evaluation of Antibacterial and Antioxidant Activities of Fluoroquinolines. *BMC Chem.* **2022**, *16* (1), No. 1.
(30) Li, Y.; Li, Y.; Liu, X.; Yang, Y.; Lin, D.; Gao, Q. The Synthesis, Characterization, DNA/Protein Interaction, Molecular Docking and Catecholase Activity of Two Co(II) Complexes Constructed from the Aroylhydrazone Ligand. *J. Mol. Struct.* **2020**, *1202*, No. 127229.
(31) Frisch, M. J.; Trucks, G. W.; Schlegel, H. B.; Scuseria, G. E.; Robb, M. A.; Cheeseman, J. R.; Scalmani, G.; Barone, V.; Petersson, G. A.; Nakatsuji, H.; Li, X.; Caricato, M.; Marenich, A. V.; Bloino, J.; Janesko, B. G.; Gomperts, R.; Mennucci, B.; Hratchian, H. P.; Ortiz, J. V.; Izmaylov, A. F.; Sonnenberg, J. L.; Williams-Young, D.; Ding, F.; Lipparini, F.; Egidi, F.; Goings, J.; Peng, B.; Petrone, A.; Henderson, T.; Ranasinghe, D.; Zakrzewski, V. G.; Gao, J.; Rega, N.; Zheng, G.; Liang, W.; Hada, M.; Ehara, M.; Toyota, K.; Fukuda, R.; Hasegawa, J.; Ishida, M.; Nakajima, T.; Honda, Y.; Kitao, O.; Nakai, H.; Vreven, T.; Throssell, K.; Montgomery, J. A., Jr.; Peralta, J. E.et al. *Gaussian 16, Revision C. 01*; Gaussian, Inc.: Wallingford CT, 2016.
(32) Ismael, M.; Abdel-Mawgoud, A. M. M.; Rabia, M. K.; Abdou, A. Design and Synthesis of Three Fe(III) Mixed-Ligand Complexes: Exploration of Their Biological and Phenoxazinone Synthase-like Activities. *Inorg. Chim. Acta* **2020**, *505* (December 2019), No. 119443.
(33) Ali, I. A. I.; El-Sakka, S. S. A.; Soliman, M. H. A.; Mohamed, O. E. A. In Silico, In Vitro and Docking Applications for Some Novel Complexes Derived from New Quinoline Derivatives. *J. Mol. Struct.* **2019**, *1196*, 8−32.
(34) Krishnan, R.; Binkley, J. S.; Seeger, R.; Pople, J. A. Self-Consistent Molecular Orbital Methods. XX. A Basis Set for Correlated Wave Functions. *J. Chem. Phys.* **1980**, *72* (1), 650−654.
(35) Grimme, S. Calculation of the Electronic Spectra of Large Molecules. *Rev. Comput. Chem.* **2004**, *20*, 153−218.
(36) Allouche, A. Gabedit — A Graphical User Interface for Computational Chemistry Softwares. *J. Comput. Chem.* **2012**, *32*, 174−182.
(37) Qiu, X.; Janson, C. A.; Smith, W. W.; Green, S. M.; McDevitt, P.; Johanson, K.; Carter, P.; Hibbs, M.; Lewis, C.; Chalker, A.; et al. Crystal Structure of *Staphylococcus Aureus* Tyrosyl-TRNA Synthetase in Complex with a Class of Potent and Specific Inhibitors. *Protein Sci.* **2001**, *10* (10), 2008−2016.
(38) Narramore, S.; Stevenson, C. E. M. M.; Maxwell, A.; Lawson, D. M.; Fishwick, C. W. G. G. New Insights into the Binding Mode of Pyridine-3-Carboxamide Inhibitors of *E. Coli* DNA Gyrase. *Bioorg. Med. Chem.* **2019**, *27* (16), 3546−3550.
(39) Krucinska, J.; Lombardo, M. N.; Erlandsen, H.; Estrada, A.; Si, D.; Viswanathan, K.; Wright, D. L. Structure-Guided Functional Studies of Plasmid-Encoded Dihydrofolate Reductases Reveal a Common Mechanism of Trimethoprim Resistance in Gram-Negative Pathogens. *Commun. Biol.* **2022**, *5* (1), No. 459.
(40) El-Hachem, N.; Haibe-Kains, B.; Khalil, A.; Kobeissy, F. H.; Nemer, G.AutoDock and AutoDockTools for Protein-Ligand Docking: Beta-Site Amyloid Precursor Protein Cleaving Enzyme 1(BACE1) as a Case Study. In *Methods in Molecular Biology*; Springer: New York, 2017; Vol. *1598*, pp 391−403 .
(41) Damena, T.; Zeleke, D.; Desalegn, T.; B Demissie, T.; Eswaramoorthy, R. Synthesis, Characterization, and Biological Activities of Novel Vanadium(IV) and Cobalt(II) Complexes. *ACS Omega* **2022**, *7* (5), 4389−4404.
(42) El-Sonbati, A. Z.; Omar, N. F.; Abou-Dobara, M. I.; Diab, M. A.; El-Mogazy, M. A.; Morgan, S. M.; Hussien, M. A.; El-Ghettany, A. A. Structural, Molecular Docking Computational Studies and in-Vitro Evidence for Antibacterial Activity of Mixed Ligand Complexes. *J. Mol. Struct.* **2021**, *1239*, No. 130481.
(43) Balouiri, M.; Sadiki, M.; Ibnsouda, S. K. Methods for in Vitro Evaluating Antimicrobial Activity: A Review. *J. Pharm. Anal.* **2016**, *6* (2), 71−79.
(44) Kowalska-Krochmal, B.; Dudek-Wicher, R. The Minimum Inhibitory Concentration of Antibiotics: Methods, Interpretation, Clinical Relevance. *Pathogens* **2021**, *10* (2), 165.
(45) Barmpa, A.; Hatzidimitriou, A. G.; Psomas, G. Copper(II) Complexes with Meclofenamate Ligands: Structure, Interaction with DNA and Albumins, Antioxidant and Anticholinergic Activity. *J. Inorg. Biochem.* **2021**, *217* (2021), No. 111357.
(46) Van de Walle, T.; Boone, M.; Van Puyvelde, J.; Combrinck, J.; Smith, P. J.; Chibale, K.; Mangelinckx, S.; D'hooghe, M. Synthesis and

https://doi.org/10.1021/acsomega.4c05560
ACS Omega 2024, 9, 36761−36777

Biological Evaluation of Novel Quinoline-Piperidine Scaffolds as Antiplasmodium Agents. *Eur. J. Med. Chem.* **2020**, *198*, No. 112330.
(47) Bahkali, A.; Wei, J.; Deng, Y. Synthesis and Characterization of Ethylenediamine Platinum(II) Complexes Containing Thiourea Derivatives. X-Ray Crystal Structures of [Pt(En)(2-Imidazolidinethione)2](NO3)2 and [Pt(En)(1-Phenyl-2-Thiourea)-2](NO3)2. *Inorg. Chim. Acta J.* **2021**, *520* (February), No. 120302.
(48) Kumar, J.; Kumar, N.; Sati, N.; Hota, P. K. Antioxidant Properties of Ethenyl Indole: DPPH Assay and TDDFT Studies. *New J. Chem.* **2020**, *44* (21), 8960−8970.
(49) Mogana, R.; Adhikari, A.; Tzar, M. N.; Ramliza, R.; Wiart, C. Antibacterial Activities of the Extracts, Fractions and Isolated Compounds from Canarium Patentinervium Miq. Against Bacterial Clinical Isolates. *BMC Complementary Med. Ther.* **2020**, *20* (1), No. 55.
(50) Sallam, S. A.; Orabi, A. S.; Abbas, A. M. DNA Interaction with Octahedral and Square Planar Ni(II) Complexes of Aspartic-Acid Schiff-Bases. *J. Mol. Struct.* **2011**, *1006* (1−3), 272−281.
(51) Abd El-Halim, H. F.; Mohamed, G. G.; Khalil, E. A. M. Synthesis, Spectral, Thermal and Biological Studies of Mixed Ligand Complexes with Newly Prepared Schiff Base and 1,10-Phenanthroline Ligands. *J. Mol. Struct.* **2017**, *1146*, 153−163.
(52) Zhu, S.-S.; Dong, X.; Zhou, Z.-H. Mixed Ligand Oxidovanadium-(IV) Complexes: Synthesis, Spectral, Structural Characterization and Catalytic Degradations of Methyl Orange. *Inorg. Chim. Acta* **2019**, *486* (October 2018), 395−400.
(53) Abane-Merzouk, L.; Adkhis, A.; Terrachet-Bouaziz, S.; Makhloufi-Chebli, M. Synthesis, DFT/TD-DFT Theoretical Studies, Experimental Characterization, Electrochemical and Antioxidant Activity of Fe(III) Complexes of Bis (Dimethylglyoximato) Guanine. *J. Mol. Struct.* **2019**, *1186*, 413−422.
(54) Neethu, K. S.; Sivaselvam, S.; Theetharappan, M.; Ranjitha, J.; Bhuvanesh, N. S. P.; Ponpandian, N.; Neelakantan, M. A.; Kaveri, M. V. In Vitro Evaluations of Biomolecular Interactions, Antioxidant and Anticancer Activities of Nickel(II) and Copper(II) Complexes with 1:2 Coordination of Anthracenyl Hydrazone Ligands. *Inorg. Chim. Acta* **2021**, *524* (November 2020), No. 120419.
(55) Ayyannan, G.; Mohanraj, M.; Gopiraman, M.; Uthayamalar, R.; Raja, G.; Bhuvanesh, N.; Nandhakumar, R.; Jayabalakrishnan, C. New Palladium(II) Complexes with ONO Chelated Hydrazone Ligand: Synthesis, Characterization, DNA/BSA Interaction, Antioxidant and Cytotoxicity. *Inorg. Chim. Acta*, **2020**, *512* (2020). 119868.
(56) Sathyadevi, P.; Krishnamoorthy, P.; Bhuvanesh, N. S. P.; Kalaiselvi, P.; Vijaya Padma, V.; Dharmaraj, N. Organometallic Ruthenium(II) Complexes: Synthesis, Structure and Influence of Substitution at Azomethine Carbon towards DNA/BSA Binding, Radical Scavenging and Cytotoxicity. *Eur. J. Med. Chem.* **2012**, *55*, 420−431.
(57) Chai, L.-Q.; Tang, L.; Chen, L.; Huang, J. Structural, Spectral, Electrochemical and DFT Studies of Two Mononuclear Manganese (II) and Zinc (II) Complexes. *Polyhedron* **2017**, *122*, 228−240.
(58) Islas, M. S.; Martínez Medina, J. J.; Piro, O. E.; Echeverría, G. A.; Ferrer, E. G.; Williams, P. A. M. Comparisons of the Spectroscopic and Microbiological Activities among Coumarin-3-Carboxylate, o-Phenanthroline and Zinc(II) Complexes. *Spectrochim. Acta, Part A* **2018**, *198*, 212−221.
(59) Su, W. Y.; Pan, R. K.; Song, J. L.; Li, G. B.; Liu, S. G. Synthesis, Crystal Structures and Cytotoxic Activity of Two Zinc(II) Complexes Derived from Benzimidazole Derivatives. *Polyhedron* **2019**, *161*, 268−275.
(60) Sezi, S.; Varghese, R.; Vilaivan, T.; Wagenknecht, H.-A. Conformational Control of Dual Emission by Pyrrolidinyl PNA-DNA Hybrids. *ChemistryOpen* **2012**, *1* (4), 173−176.
(61) Aslkhademi, S.; Noshiranzadeh, N.; Sadjadi, M. S.; Mehrani, K.; Farhadyar, N. Synthesis, Crystal Structure and Investigation of the Catalytic and Spectroscopic Properties of a Zn(II) Complex with Coumarin-Hydrazone Ligand. *Polyhedron* **2019**, *160*, 115−122.
(62) Islas, M. S.; Martínez Medina, J. J.; Piro, O. E.; et al. Comparisons of the Spectroscopic and Microbiological Activities among Coumarin-3-Carboxylate, o-Phenanthroline and Zinc(II) Complexes. *Spectrochim. Acta, Part A* **2018**, *198*, 212−221.
(63) Kargar, H.; Ardakani, A. A.; Tahir, M. N.; Ashfaq, M.; Munawar, K. S. Synthesis, Spectral Characterization, Crystal Structure and Antibacterial Activity of Nickel(II), Copper(II) and Zinc(II) Complexes Containing ONNO Donor Schiff Base Ligands. *J. Mol. Struct.* **2021**, *1233*, No. 130112.
(64) Morgan, S. M.; El-Sonbati, A. Z.; Eissa, H. R. Geometrical Structures, Thermal Properties and Spectroscopic Studies of Schiff Base Complexes: Correlation between Ionic Radius of Metal Complexes and DNA Binding. *J. Mol. Liq.* **2017**, *240*, 752−776.
(65) Indira, S.; Vinoth, G.; Bharathi, M.; Shanmuga Bharathi, K. Synthesis, Spectral, Electrochemical, in-Vitro Antimicrobial and Antioxidant Activities of Bisphenolic Mannich Base and 8-Hydroxyquinoline Based Mixed Ligands and Their Transition Metal Complexes. *J. Mol. Struct.* **2019**, *1198*, No. 126886.
(66) Zordok, W. A.; Sadeek, S. A. Synthesis, Spectroscopic Characterization, Biological Studies and DFT Calculations on Some Transition Metal Complexes of NO Donor Ligand. *J. Mol. Struct.* **2018**, *1158*, 205−220.
(67) Badwaik, V. B.; Deshmukh, R. D.; Aswar, A. S. Transition Metal Complexes of a Schiff Base: Synthesis, Characterization, and Antibacterial Studies. *J. Coord. Chem.* **2009**, *62* (12), 2037−2047.
(68) Krasnovskaya, O.; Naumov, A.; Guk, D.; Gorelkin, P.; Erofeev, A.; Beloglazkina, E.; Majouga, A. Copper Coordination Compounds as Biologically Active Agents. *Int. J. Mol. Sci.*, **2020**, *21* (11). 3965.
(69) Sumalatha, V.; Daravath, S.; Rambabu, A.; Ramesh, G.; Shivaraj. Antioxidant, Antimicrobial, DNA Binding and Cleavage Studies of Novel Co(II), Ni(II) and Cu(II) Complexes of N, O Donor Schiff Bases: Synthesis and Spectral Characterization. *J. Mol. Struct.* **2021**, *1229*, No. 129606.
(70) Belkhir-Talbi, D.; Ghemmit-Doulache, N.; Terrachet-Bouaziz, S.; Makhloufi-Chebli, M.; Rabahi, A.; Ismaili, L.; Silva, A. M. S. Transition-Metal Complexes of N,N′-Di(4-Bromophenyl)-4-Hydroxycoumarin-3-Carboximidamide: Synthesis, Characterization, Biological Activities, ADMET and Drug-Likeness Analysis. *Inorg. Chem. Commun.* **2021**, *127* (March), 1−12.
(71) Hamdani, S. S.; Khan, B. A.; Ahmed, M. N.; Hameed, S.; Akhter, K.; Ayub, K.; Mahmood, T. Synthesis, Crystal Structures, Computational Studies and α-Amylase Inhibition of Three Novel 1,3,4-Oxadiazole Derivatives. *J. Mol. Struct.* **2020**, *1200*, No. 127085.
(72) Azam, M.; Al-Resayes, S. I.; Trzesowska-Kruszynska, A.; Kruszynski, R.; Shakeel, F.; Soliman, S. M.; Alam, M.; Khan, M. R.; Wabaidur, S. M. Zn(II) Complex Derived from Bidentate Schiff Base Ligand: Synthesis, Characterization, DFT Studies and Evaluation of Anti-Inflammatory Activity. *J. Mol. Struct.* **2020**, *1201*, No. 127177.
(73) Stracy, M.; Wollman, A. J. M.; Kaja, E.; Gapinski, J.; Lee, J. E.; Leek, V. A.; McKie, S. J.; Mitchenall, L. A.; Maxwell, A.; Sherratt, D. J.; et al. Single-Molecule Imaging of DNA Gyrase Activity in Living *Escherichia Coli*. *Nucleic Acids Res.* **2019**, *47* (1), 210−220.
(74) He, J.; Qiao, W.; An, Q.; Yang, T.; Luo, Y. Dihydrofolate Reductase Inhibitors for Use as Antimicrobial Agents. *Eur. J. Med. Chem.* **2020**, *195*, No. 112268.
(75) Srinivasan, B.; Tonddast-Navaei, S.; Roy, A.; Zhou, H.; Skolnick, J. Chemical Space of *Escherichia Coli* Dihydrofolate Reductase Inhibitors: New Approaches for Discovering Novel Drugs for Old Bugs. *Med. Res. Rev.* **2019**, *39* (2), 684−705.
(76) Ndagi, U.; Kumalo, H. M.; Mhlongo, N. N. A Consequence of Drug Targeting of Aminoacyl-TRNA Synthetases in *Mycobacterium tuberculosis*. *Chem. Biol. Drug Des.* **2021**, *98* (3), 421−434.

https://doi.org/10.1021/acsomega.4c05560
ACS Omega 2024, 9, 36761−36777